Presentation
& conference tips

Isabelle Grenier
Université Paris Diderot & CEA Saclay
Institut Universitaire de France

Outline

- message pitches
- posters
- viewgraphs
- figure tips
- conference goals

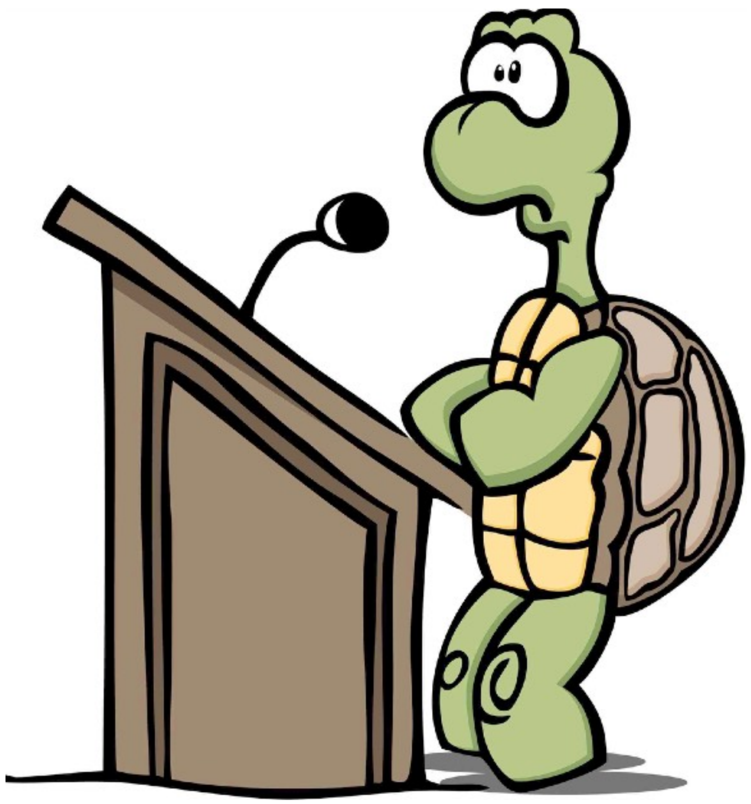

Message pitch

- what is your research topic?
  - what must the audience know?
  - what were you hoping to find out and why?
- which route did you take?
- what have you found?
- why is that important?

- oral presentation
  - logical style
  - highlights at the end for questions

context + definitions

data + methods

results

open questions + legacy value

- poster presentation
  - journalistic style
  - to "sell" your work

2-line result synopsis

abstract with context & results

data + methods frame

result plots + captions

legacy + future frame

compare styles

- in Science journal:

The origin of Galactic cosmic rays is a century-long puzzle. Indirect evidence points to their acceleration by supernova shockwaves, but we know little of their escape from the shock and their evolution through the turbulent medium surrounding massive stars. Gamma rays can probe their spreading through the ambient gas and radiation fields. The Fermi Large Area Telescope (LAT) has observed the star-forming region of Cygnus X. **The 1- to 100-GeV images reveal a 50-parsec-wide cocoon of freshly accelerated cosmic rays that flood the cavities carved by the stellar winds and ionization fronts from young stellar clusters.** It provides an example to study the youth of cosmic rays in a superbubble environment before they merge into the older Galactic population.

Ackermann et al. 2011

- in the press

New images link cosmic rays to an enormous bubble of gas blown by hot, young stars, implying that these mysterious high- energy particles may be made in the same factories where stars are born.

Cosmic rays have puzzled astronomers since they were discovered nearly a century ago. Most are protons and other atomic nuclei. They bombard our planet from all directions, travelling at close to the speed of light. Where cosmic rays come from is unknown.
Astronomers suspect that supernova explosions boost them to such high speeds. Supernovae happen most often in dense clouds of gas and dust where stars between 10 and 50 times the mass of the sun are born and die …

New Scientist 2011

Posters

Poster preparation

- clear, simple, attractive layout
  - check the size on the conference web site
  - strip cartoon style
    - from one succinct frame to another in a logical fashion
    - mostly charts or graphs with short captions rather than text
    - guide the reader with arrows or numbers
  - huge fonts
  - add “preliminary” on unpublished figures
  - leave empty space
- insert
    - an ID picture + email/SMS link for people to find you
    - institute logos
    - acknowledgments & project grants
- prepare
  - a $\leq$ 3-sentence oral synopsis to engage passers-by
  - short answers for likely questions
- give handouts
  - copy or link to the poster or publication

example

- good title
- preliminary vs. future work
- simple flow

- text length & complexity, many acronyms
- no abstract, essential info missing
- conclusions hidden, impact missing

The seed factor: how a combination of four observables can unveil the location of the blazar GeV emission.

xxxxxxxx

Introduction.

The location in FSRQs in which GeV emission is produced is an open question. In leptonic scenarios, GeV radiation is most likely emitted via inverse Compton scattering of photons in the broad-line region (BLR) or in the molecular torus (MT), called external Compton (EC) scattering. We have developed a diagnostic criterion to deterine in which of these two locations GeV emission is produced for a given SED. We term this criterion the "seed factor" (SF). Multiwavelength emission from the BLR and the MT both produce characteristic values of the seed factor.

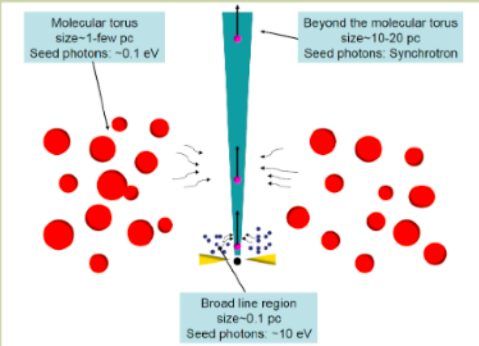

Figure 1: Blazar diagram showing distances of MT and BLR.

Derivation.

The peak energies (in units of electron rest mass energy) of synchrotron and external Compton scattering are, respectively,

$$\epsilon_s = \frac{B}{B_{cr}}\gamma^2\delta \quad (1)$$

$$\epsilon_c = \frac{4}{3}\epsilon_0\gamma_b^2\delta^2 \quad (2)$$

where ϵ_0 is the characeristic energy of the external seed photons.

Eqn. 2 is valid if the electron scattering takes place in the Thompson regime. Scattering is in the Thompson regime if $\sqrt{\epsilon_c\epsilon_0} \lessapprox 1$. The highest energy possible for external seed photons are UV emission-line photons which have $\epsilon_0 \approx 10^{-4}$. Thus scattering is in Thompson regime if $\nu_c \lessapprox 10^{24}$ Hz. Which is generally true, since for powerful blazars $\langle\nu_c\rangle \approx 10^{22}$ Hz.

Dividing Eqn. 2 by Eqn. 1 and solving for $\frac{B}{\delta}$,

$$\frac{B}{\delta} = \frac{4\epsilon_0\epsilon_s B_{cr}}{3\epsilon_c} \quad (3)$$

To create a diagnostic based solely on observables, we now consider the Compton dominance. This is,

$$k = \frac{L_c}{L_s} = \frac{32\pi\delta^2 U_0}{3B^2} \quad (4)$$

Solving for $\frac{B}{\delta}$ and equating to Eq. 3, we find,

$$\frac{U_0^{1/2}}{\epsilon_0} = 3.2\times10^4\ \mathrm{G}\frac{k_1^{1/2}\nu_{s,13}}{\nu_{c,22}} \quad (5)$$

where k_1 is the Compton dominance in units of 10, $\nu_{s,13}$ is the synchrotron peak in units of 10^{13} Hz, and $\nu_{c,22}$ is the EC peak in units of 10^{22} Hz. It is Eqn. 6 which we term the seed factor.

Reverberation mapping of radio quiet finds that $R_{BLR} \approx 10^{17}L_{d,45}^{1/2}$ [1]. Assuming this holds for powerful blazars and that $\xi_{BLR} \sim 0.1$ [2], $U_0 \approx 2.6\times10^{-2}$ erg cm^{-3}. The BLR SED can be approximated by a blackbody (BB) with peak at $\epsilon_0 \approx 3\times10^{-5}$ [3]. Thus $SF_{BLR} \sim 5.5\times10^3$ G.

In the MT, reverberation mapping [4,5] and NIR interferometric studies [6] of radio quiet sources find $R_{MT} \approx 10^{18}L_{d,45}^{1/2}$. Adopting $\epsilon_0 = 5.7\times10^{-7}$ (a BB of $T = 1200$ K) and $\xi_{MT} \sim 0.2$ [7] we obtain $SF_{MT} \sim 4\times10^4$ G.

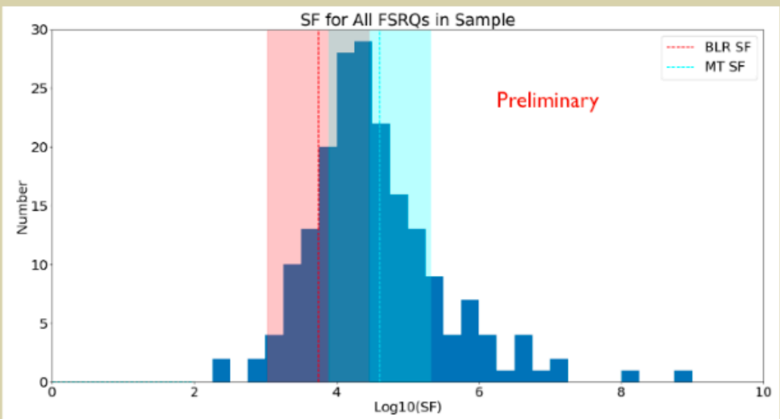

Figure 2: Histogram of seed factors for all FSRQs in sample.

Preliminary Work.

We have derived the SF for four samples (Arsioli+ (2018) [8], MOJAVE [9], LBAS [10], DSSB [11]). A histogram of all the SFs from these samples can be seen in Fig. 2. A histogram for the MOJAVE sample can be seen in Fig. 4. The MOJAVE sample has been singled out due to the completeness of the MOJAVE sample.

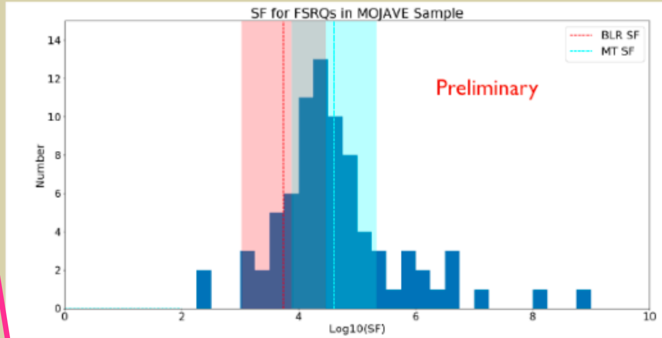

Figure 3: Histogram of seed factors of cumulative historical data from the ASDC SED Builder for MOJAVE sample FSRQs.

Combining all four of these samples does not show a strong preference for either the BLR or the MT. The MT may be favored slightly in the MOJAVE sample. The MOJAVE sample is, however, in close agreement with the total distribution.

Our results show that emission is consistent with EC emission. There may be emission outside of the BLR or MT, as indicated by large values of the SF. More accurate measurements of the peak frequencies and luminosities can provide better discrimination between emission locations.

description of next test, not of the impact or usefulness of such a new diagnostic

References.

1. Bentz et al. 2013, ApJ 767 149
2. Ghisellini & Tavecchio 2009, MNRAS 397 985
3. Tavecchio et al. 2008, MNRAS 386 945
4. Suganuma et al. 2006, ApJ 639 46
5. Pozo Nuñez et al. 2014, A&A 561 L8
6. Kishimoto et al. 2011, A&A 536 78
7. Hao, et al. 2005, AJ 129 1795
8. Arsioli and Polenta 2018, arXiv:1804.03703
9. Lister et al. 2009 AJ 137.3718L
10. Abdo et al. 2010 ApJ 716 30A
11. Krauß et al. 2016 A&A 591.A130K

Acknowledgements.

This work is supported by NASA/Fermi Grant #00011640.

example

- no guiding key words for the sections
- summary at the bottom
- lengthy tables instead of graphs relating the listed variables

Optical, ultraviolet, infrared follow-ups of *Fermi* pulsars

NUI Galway
OĖ Gaillimh

XXXXXXXX

Abstract: The wealth of pulsar detections by *Fermi* paved the way to multi-wavelength follow-ups to extend the characterisation of their spectral and timing properties. Being pulsars quite faint in the optical, ultraviolet, and infrared, this has required observations with 8m-class telescopes and with the *HST*. In this poster we briefly summarise 10 years of follow-ups of *Fermi* pulsars in these spectral regions.

The copious detection of γ-ray pulsars by the Fermi Large Area Telescope (LAT), with 216 of them identified since the launch of the satellite in 2008, makes them the largest class of identiifed Galactic γ-ray sources. The harvest of pulsar γ-ray detections has fostered the interest on their multi-wavelength studies, especially in the X-rays and in the optical (O), ultraviolet (UV), infrared (IR) -**UVOIR** for short- to characterise their spectral energy distribution (SED) and study the interplay between different emission mechanisms. Pulsars are intrinsically very faint in the UVOIR domain, where they are detected only through the emission of synchrotron radiation from relativistic particles in their magnetosphere (power law spectra with α =0-1) and/or thermal radiation from their hot (brightness temperatures 0.1-1 MK) surface. Thus, they are challenging targets in the UVOIR and very few of them have been identified.

TABLE 1: γ-ray pulsars Identified *before* the launch of *Fermi*

NAME	P(ms)		Log(Age)	Log(Edot)	Mag		Band	D(kpc)	Ref
Crab	33	[$P_{OPT,UV,IR}$]	3.10	38.65	V=16.6	[36 inch]	UVOIR	2	Cocke et al., 1969, Nature, 221, 525
PSR B1509-58	151		3.19	37.25	R=25.7	[VLT]	OIR	4.2	Wagner & Seifert, 2000, ASP, 202, 315
PSR B0540-69	50	[$P_{OPT,UV}$]	3.23	38.69	V=22.5	[NTT]	UVOIR	48.9	Caraveo et al., 1992, ApJ, 395, 103
Vela	89	[$P_{OPT,UV}$]	4.05	36.84	V=23.6	[Blanco]	UVOIR	0.287	Lasker, 1976, ApJ, 203, 193
PSR B0656+14	384	[$P_{OPT,UV}$]	5.05	34.58	V=25	[NTT]	UVOIR	0.288	Caraveo et al., 1994, ApJ, 422, L87
Geminga	237	[$P_{OPT,UV}$]	5.53	34.51	V=25.5	[NTT]	UVOIR	0.250	Bignami et al., 1993, Nature, 361, 704
PSR B1055-52	197		5.73	34.48	V=25.5	[HST]	UVO	0.350	Mignani et al., 1997, ApJ, 474, L51
PSR J0437-5715	5.96		9.69	33.58	V~25^{extr}	[HST]	UV	0.139	Kargaltsev et al., 2004, ApJ, 602, 372

Till recently, the γ-ray pulsars identified in in at least one of the UVOIR energy bands were mostly those originally detected by *SAS-2* and *COS-B* in the 1970s/1980s (the **Crab** and **Vela** pulsars, **Geminga**) or by the *Compton Gamma-ray Observatory* (**PSR B0656+14, PSR B1055-52, PSR B1509-58**). PSR B1706-44 and PSR B1951+32 are the only two *Compton* γ-ray pulsars that are still unidentified in the UVOIR. Table summarises all γ-ray pulsars identified in at least one UVOIR band before the launch of *Fermi*, mostly in the 1990s. The Large Magellanic Cloud **PSR B0540-69** and the old, recycled milli-second pulsar (MSP) **PSR J0437-4715** [both marked in red] were identified well ahead of their detection as γ-ray pulsars by *Fermi*. PSR J0437-4715 is also the only binary MSP identified in the UVOIR. There are only five γ-ray pulsars (Crab, Vela, PSR B0540-69, Geminga, PSR B0656+14) detected in all the UVOIR bands (Mignani et al. 2018a, submitted to ApJ, arXiv:1809.10805). The pulsars marked as [$P_{OPT,UV}$] are those pulsating in the optical and in the UV. Only the Crab, [$P_{OPT,UV,IR}$], also pulsates in the IR.

TABLE 2: γ-ray pulsars Identified *after* the launch of *Fermi*

NAME	P(ms)	Log(Age)	Log(Edot)	Mag		Band	D(kpc)	Ref
PSR J0205+6449	65	3.73	37.43	r'=26.2	[Gem]	O	3.2	Moran et al., 2013, MNRAS, 436, 401
PSR J1357-6429	166	3.86	36.49	J=23.5	[VLT]	IR	2.4	Zyuzin et al., 2016, MNRAS, 455, 1746
PSR J1741-2054	413	5.58	33.97	V=25.3	[VLT]	O	0.38	Mignani et al., 2016, ApJ, 825, 151
PSR J2124-3358	4.93	9.58	33.83	B=27.5	[HST]	UVO	0.41	Rangelov et al., 2017, ApJ, 835, 264

UVOIR candidate counterparts to γ-ray pulsars have been identified after the launch of *Fermi* exploiting the collecting power of 8m-class ground-based telescopes deployed in the late 1990s and the UV sensitivity of the *HST*. **PSR J0205+6449** was identified using archival data from the Gemini North telescope but the other three pulsars were identified thanks to dedicated follow-ups with the VLT (**PSR J1357-6429**, **PSR J1741-2054**) and the *HST* (**PSR J2124-3358**). Table 2 summarises the new candidate identifications, with PSR J2124-3358 being the first isolated MSP identified in the UVOIR. For none of them UVOIR pulsations have been detected yet, both owing to the relatively recent counterpart identification and to the paucity of instruments for high-time resolution observations. This γ-ray pulsar identification rate [0.4 yr^{-1}] compares favourably with that before the launch of *Fermi* [~0.2 yr^{-1}] but not much so when considering the factor of ~30 increase in the number of γ-ray pulsars, even accounting for the few years needed for the identification process. The identification effort continued restlessy, though.

TABLE 3: γ-ray pulsars Observed *after* the launch of *Fermi*

NAME	P(ms)	Log(Age)	Log(Edot)	Mag		D(kpc)	Ref
PSR J0007+7303	316	4.14	35.65	r'>27.6	[GTC]	1.4	Mignani et al., 2013, MNRAS, 430, 1354
PSR J2021+3651	104	4.23	36.53	r'>27.2	[GTC]	1	Kirichenko et al., 2015, ApJ, 802, 17
PSR J1907+0602	106	4.29	36.44	V>26.9	[VLT]	2.58	Mignani et al., 2016b, MNRAS, 463, 2932
PSR J1048-5832	123	4.30	36.30	V>27.6	[VLT]	2.7	Razzano et al., 2013, MNRAS, 426, 3636
PSR J0631+1036	287	4.64	35.23	g'>27	[GTC]	1.0	Mignani et al., 2016a, MNRAS, 451, 4317
PSR J0633+0632	297	4.77	35.08	g'>27.3	[GTC]	<8.7	Mignani et al., 2016a, MNRAS, 451, 4317
PSR J0248+6021	217	4.79	35.32	g'>27.3	[GTC]	2.0	Mignani et al., 2016a, MNRAS, 451, 4317
PSR J1809-2332	146	4.83	35.63	V>27.6	[VLT]	1.7	Mignani et al., 2016b, MNRAS, 463, 2932
PSR J1028-5819	91	4.95	35.92	V>25.3	[VLT]	2.3	Mignani et al., 2012, A&A, 543, 130
PSR J1846+0919	225	5.55	34.53	g'>27.0	[GTC]	1.4	Mignani et al., 2018b, MNRAS, 478, 332
PSR J0357+3205	444	5.74	33.76	g'>28.1	[GTC]	0.5	Kirichenko et al., 2014, A&A, 564, 81
PSR J2043+2740	96	6.08	34.74	g'>27.2	[GTC]	1.48	Mignani et al., 2018b, MNRAS, 478, 332
PSR J2055+2539	319	6.09	33.69	g'>26.8	[GTC]	0.6	Mignani et al., 2018b, MNRAS, 478, 332

Follow-up observations of *Fermi* γ–ray pulsars continued on the [supposedly] best candidates but were hampered in some cases by the uncertain distance estimate, without known radio parallaxes, by the lack of accurate radio or *Chandra* coordinates, and by the uncertain extinction determination, which relies on X-ray observations to infer the N_H from the spectral fits. Thus, the chances of success of UVOIR follow-ups depend on coordinated radio/X-ray observations, which also imposes a physiological delay in the identification process. In most cases it was possible to set deep constraints on the UVOIR flux, though. Table 3 summarises follow-ups of γ-ray pulsars with 8m-class telescopes (optical band only). In all cases the detection limits are between magnitude ~27 and 28, i.e. close to the limits of current facilities. A compilation of detection limits for γ-ray pulsars observed prior to their detection by *Fermi* can be found in the Second γ-ray Pulsar Catalogue (Abdo et al. 2013, ApJS, 208, 17). As it can be seen (Table 2, 3), most of the observational effort has relied on European telescopes (GTC,VLT), with *HST* focussed on follow-ups of identified pulsars (e.g., Mignani et al. 2018a) and Subaru, Keck, Gemini, LBT essentially unused – resources to be exploited in the future.

Summary: The UVOIR follow-ups of γ-ray pulsars show that the SEDs commonly feature breaks between the high and low-energy power-law spectra and do not follow a unique template even in pulsar with similar characteristics (e.g., Mignani et al. 2016), suggesting that the topology of the emission regions, the beaming and viewing geometry play an important role. UVOIR timing observations, in parallel to X and γ-ray ones, are crucial to address this issue. In relative terms, the UVOIR luminosity is a small fraction of the X and γ-ray ones, where the ratio span from -3.2 to -4.7 [in logarithmic units] in the X-rays and from -2.6 to -7.2 in γ-rays showing that in the latter case the relative yield is more variable, perhaps owing to a different emission configuration between the X and γ-rays. The UVOIR pulse profiles are, generally, not aligned with the γ-ray ones, with the exception of the Crab pulsar and PSR B0540-69, where they feature a remarkable alignment and similarity. Among the identified γ-ray pulsars, **PSR B1055-52** and **PSR J1741-2054** are, probably, the next best targets to search for optical/UV pulsations.

example

- clear, attractive layout
- text too wordy
- redundant conclusions & abstract
- curve drawings to be improved

CLEMSON UNIVERSITY

2FHL J0826.1-45.00: Discovery of a new VHE Galactic Accelerator

CLEMSON UNIVERSITY

XXXXXXXXX

ABSTRACT

The discovery of a very high energy (VHE) Galactic gamma-ray source was recently observed at energies above 50GeV using the Large Area Telescope (LAT) on board *Fermi*. This object, 2FHL J0826.1-4500, displays one of the hardest >50 GeV spectra (photon index~1.6) in the 2FHL sample, and a follow-up observation with XMM-*Newton* led to the discovery of diffuse, soft thermal emission at the position of the gamma ray source. A detailed analysis of the available multi-wavelength data led to the finding that this source is located on the Western edge of the Vela supernova remnant (SNR): the observations and the spectral energy distribution modeling support a scenario where 2FHL J0826.1-4500 is the byproduct of an interaction between the front shock of the SNR and a neutral Hydrogen cloud. If confirmed, this shock-cloud interaction would make 2FHL J0826.1-4500 a promising candidate for efficient particle acceleration.

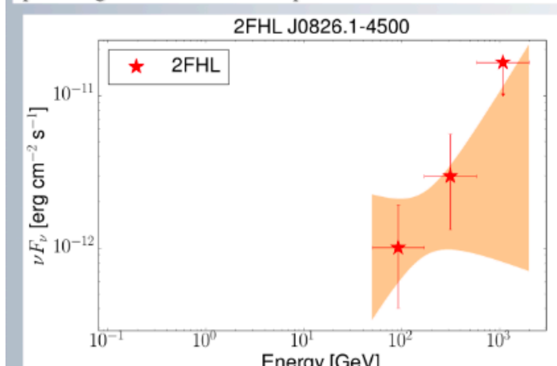

Fig 1: The gamma-ray spectrum of 2FHL J0826.1-4500. The spectrum is very hard with Γγ =1.6 ± 0.3.

MISSION

2FHL J0826.1-4500 presents a particularly hard γ-ray spectrum with photon index $\Gamma\gamma = 1.6 \pm 0.3$ and a maximum energy photon of ~412GeV detected by the LAT (see figure 1 above). The source is compact and shows no clear evidence of extended emission beyond the point spread function of the *Fermi*-LAT in this energy range. To further investigate the properties of this intriguing VHE object, we were granted a 20ks XMM-*Newton* follow-up observation. XMM-*Newton* has the largest effective area in the 0.5–10keV band among all the X-ray telescopes, therefore being the most effective instrument to detect faint, diffuse X-ray emission along the Galactic plane, like the one commonly observed in PWNe and SNRs.

REFERENCES

☼ Atwood, W., Albert, A., Baldini, L. et al. 2013a, ArXiv e-prints [1303.3514] ☼ Atwood, W. B., Baldini, L., Bregeon, J., et al. 2013b, ApJ, 774, 76 ☼ Ackermann, M., Ajello, M., Baldini, L., et al. 2017, ApJ, 843, 139 ☼ Dubner, G. M, Green, A. J., Goss, W. M., Bock, D. C.-L., & Giacani, E. 1998, AJ, 116, 813 ☼ Duncan, A. R., Stewart, R. T., Haynes, R. F., & Jones, K. L., 1996, MNRAS, 280, 252 ☼ H.E.S.S. Collaboration, Abdalla, H., Abramowski, A., et al. 2018b, A&A, 612, A1 ☼ Murphy, T., Mauch, T., Green, A., et al. 2007, MNRS, 382, 382

*e − mail: jeagle@clemson.edu

SPECTRAL ANALYSIS

In the figure below (Fig 2, left panel) we show the smoothed 0.5-2keV image of 2FHL J0826.1-4500 as seen with the MOS2 camera mounted on XMM-*Newton*. Faint, diffuse X-ray emission is evident with extension of roughly 15'. X-ray emission is spatially coincident with an optical filament visible in Hα (figure 2, right panel). Analysis of X-ray emission reveals it to be soft with no significant emission detected above 2keV. Spectral fitting was performed to characterize observed emission. Due to low signal-to-noise, we chose to model both the background and source emission (rather than subtracting background emission which would lead to poor statistics with such few photon counts). Background emission was modeled taking into account both instrumental and astrophysical background. Spectral fitting was performed with the most recent update of HEASOFT software with corresponding calibration files for the XMM-*Newton* telescope.

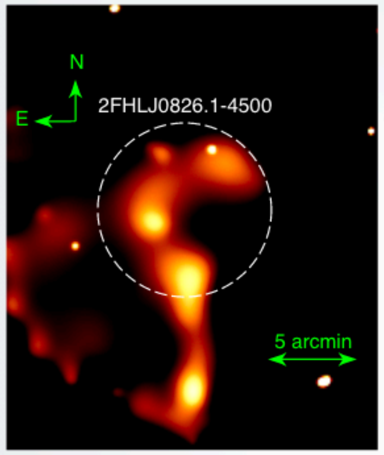

Fig 2: Left: Smoothed 0.5-2keV image of 2FHL J0826.1-4500 created using CIAO `csmooth` tool using the faster fourier transforms convolution method and a Gaussian convolution kernel set to 3. Right: X-ray emission countours overlaid on an Hα image of the region of 2FHL J0826.1-4500. In both images, the white dashed circle marks the FERMI-LAT position, r=4'.

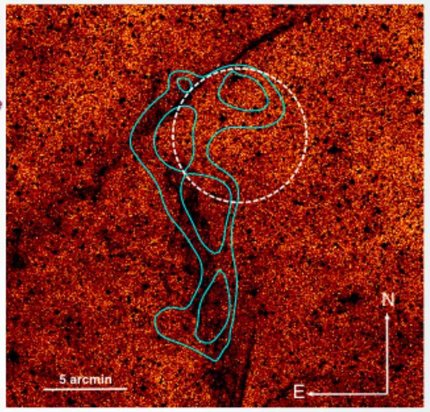

SPECTRAL ANALYSIS RESULTS

A thermal emission scenario was found to be statistically preferred over a non-thermal scenario (`mekal` vs. power law) with a best-fit temperature of $kT = 0.60 \pm {}^{0.11}_{0.60} keV$ that can be interpreted as an upper limit of $kT < 0.72keV$. Upon a multi-wavelength analysis, we link this source with the front shock of the Vela SNR, located on the Western edge, and is located at ~1.5° SW of the Vela Pulsar. Additionally, it is found that an HI cloud is seen to be spatially and morphologically coincident with 2FHL J0826.1-4500 (Fig 3, right panel) . A deeper investigation leads us to believe the combined gamma-ray, X-ray, optical, and radio data depicts a scenario of interaction between the Vela SNR forward shock and the HI cloud.

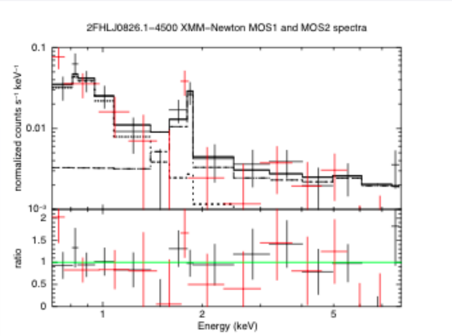

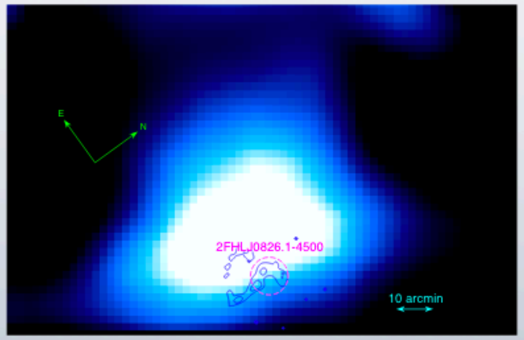

Fig 2 (above, left): XMM-Newton MOS1 (black) and MOS2 (red) data of 2FHL J0826.1-4500 and the best-fit model obtained using `mekal`. The best-fit model (solid black line), the instrumental background (dashed black line) and the combination of source and astrophysical background (dotted black line) are plotted. PN data was removed for clarity. (above, right): HI 21cm radio map integrated between 29.7 and 35.3 $\frac{km}{s}$ indicating the location of 2FHL J0826.1-4500 with respect to the HI cloud with blue contours for reference of shock structure and location.

SED MODELING

The multi-wavelength information available can be combined to build a picture of the broadband spectral characteristics of the region. The data are shown below with upper limits from 843MHz and 2.4GHz radio emission, soft X-ray emission, and TeV gamma-ray emission. Assuming a distribution of accelerated particles in momentum to be:

$$\frac{dN_i}{dp} = a_i p^{-\alpha_i} \exp(\frac{p}{p_{0,i}})$$

Where i is either proton or electron population, and α_i and $p_{0,i}$ are the spectral index and the exponential cutoff momentum of the distributions, respectively. a_i is set using the total energy in relativistic particles and the electron to proton ratio as input parameters, together with the spectral shape of the distributions. For non-thermal radiation from the particle distributions we have used pion-decay emission, synchrotron and inverse Compton (IC) emission, and non-thermal bremsstrahlung emission. The model (Fig 3) establishes the range of some physical parameters that would result in the observed *Fermi*-LAT emission as well as complying with the upper-limits at other wavelengths.

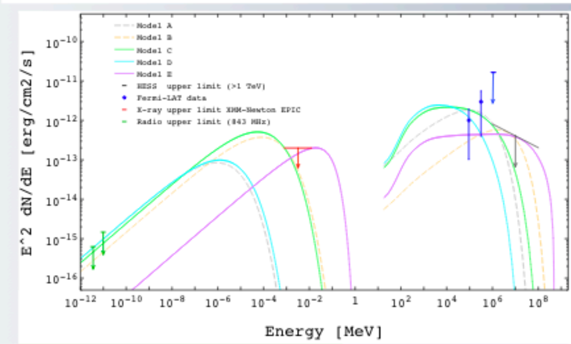

		p_0 (TeV/c)	$B_{2,max}$ (μG)	$n_H \times E_{CR,p}$ (10^{48} erg/cm³)	$E_{CR,e}$ (10^{44} erg)
Leptonic	A	5	3	–	9
	B	30	9	–	1
Hadronic	C	10	50	6	–
	D	1	50	6	–
	E	600	10	1	–

Fig 3: Spectral energy distribution (SED) for various scenarios constrained to upper limits of available data across the electromagnetic spectrum. Models A (gray dashed line) and B (yellow dashed line) demonstrate resultant gamma-ray spectrum of radiation from relativistic electrons. Models C (solid green), D (solid cyan), and E (solid purple) demonstrate resultant spectrum of radiation from a hadronic population. Table shown provides the input model parameters for each SED model.

CONCLUSIONS

Data presented for 2FHL J0826.1-4500 supports a shock-cloud interaction scenario on the western edge of the Vela SNR. Multi-wavelength data suggests the FS of the SNR is interacting with a small HI cloud. This makes 2FHL J0826.1-4500 a candidate for CR acceleration. If the hadronic models prove to be most realistic in characterizing 2FHL J0826.1-4500, not only is the location a likely site of efficient particle acceleration, but also poses as a possible site of fresh CR acceleration. Future work to confirm this includes studying the physical conditions (e.g. velocity, direction, elemental composition) of the shock which will help us understand the shock's kinematics and thus can provide clues to whether 2FHL J0826.1-4500 may be a site generating fresh CRs or is instead a re-acceleration mechanism.

example

- clear & attractive layout (numbering)
- punch line
- obvious conclusions
- graphs too small

Optimizing Multi-Wavelength Blazar Studies Through *Fermi*-LAT and *Swift* Synergy

XXXXXXX

Methods

1. Sort through *Fermi* LAT's Monitored Source List (fermi.gsfc.nasa.gov/ssc/data/access/lat/msl_lc/) with a photon flux, $\Phi \geq 1.0 \times 10^{-6} \frac{(E>100MeV)photons}{cm^2 s}$, picking out sources that flared prior to 2017 and had significant and visually interesting activity. We found that 110/158 were of interest.

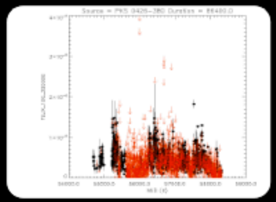

Fermi-LAT light curve example of PKS 0426-380 (red arrows represent upper limits)

2. Determine if *Fermi* sources had *Swift* ToO follow ups by searching in online *Swift* ToO archive (https://www.swift.psu.edu/secure/toop/summary.php).
3. Analyze fits file data with one another. Over-plot light curves to compare with one another

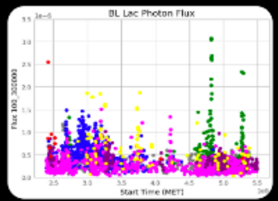

Published BL Lac sources plotted in python for comparison analysis

4. Perform Bayesian Block analysis to determine flare durations in each source

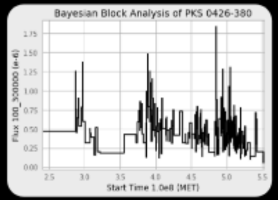

Bayesian Block analysis of PKS 0426-380 helping to provide insight into flare duration

5. Determine which blazar classifications, FSRQs or BL Lacs, are most abundantly published (using info from *Fermi* LAT 4 year Catalog)
6. Determine which type of flaring sources are more likely to result in publications by searching for publications in the SAO/NASA ADS Astronomy Query (http://adsabs.harvard.edu/abstract_service.html).

Summary

Swift ToO observations of flaring *Fermi*-LAT blazars are likely to result in publications for historically active sources and high-photon-flux sources.

Abstract

Blazar flares seen by the *Fermi Gamma-Ray Space Telescope* Large Area Telescope (*Fermi* LAT) are often followed up by Target of Opportunity (ToO) requests to the *Neil Gehrels Swift Observatory (Swift)*. Using flares identified in the daily light curves of *Fermi* LAT Monitored Sources, we investigated which follow-up *Swift* ToO requests resulted in refereed publications. The goal was to create criteria of what *Swift* should look for in following up a *Fermi*-LAT gamma-ray flare. Parameters tested were peak gamma-ray flux, flare duration (based on a Bayesian Block analysis), type of AGN (BL Lac or FSRQ), and pattern of activity (single flare or extensive activity). We found that historically active sources and high-photon-flux sources result in more publications, deeming these successful *Swift* ToOs, while flare duration and type of AGN had no impact on whether or not a ToO led to a publication.

83% of interesting *Fermi* observations have *Swift* counterparts (91/110)

35% of *Fermi*-*Swift* sources have general publications (32/91)

19% of original *Fermi* observations have publications with specified *Swift* ToOs. (21/110)

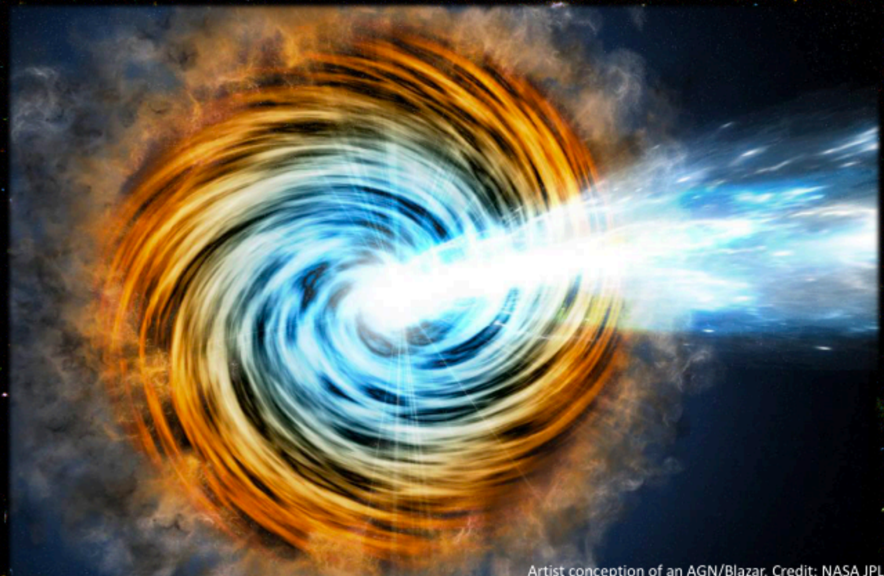

Artist conception of an AGN/Blazar. Credit: NASA JPL

Hypothesis vs. Results

- The **left** graph represents a *Fermi*-LAT light curve hypothesized to produce publications: single bright flare.

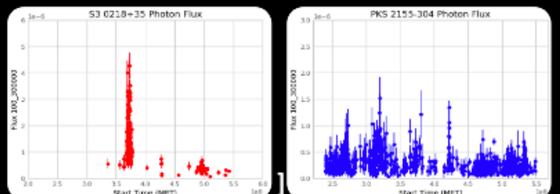

FSRQ S3 0218+35, showing one steep, single spike in flux

BL Lac PKS 2155-304, showing historic and oscillating activity

- The **right** graph represents a standard *Fermi* light curve that actually produced publications.

Conclusions

1. Higher flux flares were published more than lower flux flares
   A. $\overline{\Phi} = 8.6 \times 10^{-6} \frac{photons}{cm^2}/s$ for published *Fermi-Swift* sources. Median value = 2.4(e-6)
   B. $\overline{\Phi} = 2.2 \times 10^{-6} \frac{photons}{cm^2}/s$ for non-published *Fermi*-*Swift* sources. Median value= 2.0(e-6)
   C. $\overline{\Phi} = 1.2 \times 10^{-6} \frac{photons}{cm^2}/s$ for *Fermi*-LAT sources that did not have a *Swift* follow-up. Median value = 1.1(e-6)
2. 87.5% (7/8) of *Fermi*-LAT sources with flux $\geq 8.0 \times 10^{-6} \frac{photons}{cm^2}/s$ had publications with *Swift* ToO observations (In the 8th case, a ToO was not possible due to a *Swift* sun angle constraint).
3. 18.4% (14/76) of sources with a max flux between 1.0-3.0 (e-6) had publications with *Swift* ToO observations.
4. Unlike the initial hypothesis, historically active and or oscillating sources resulted in more publications rather than one single, steep spike in the flux.
5. 4 BL Lacs, 12 FSRQs, and 4 uncertain blazars published.

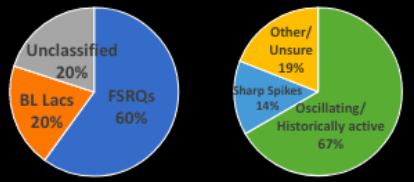

6. 14 sources were oscillating/historically active, 2 sources had sharp spikes (both FSRQs), and 3 were somewhat hybrids.
7. Published sources had a higher average number of flares at 2.6 than non-published sources at 1.7.
8. Durations of flares were highly variable, meaning that flare duration should not necessarily matter when accepting a ToO.

example

- clear & numbered structure
- clear graphs
- punchy questions & conclusions
- contacts & QR code

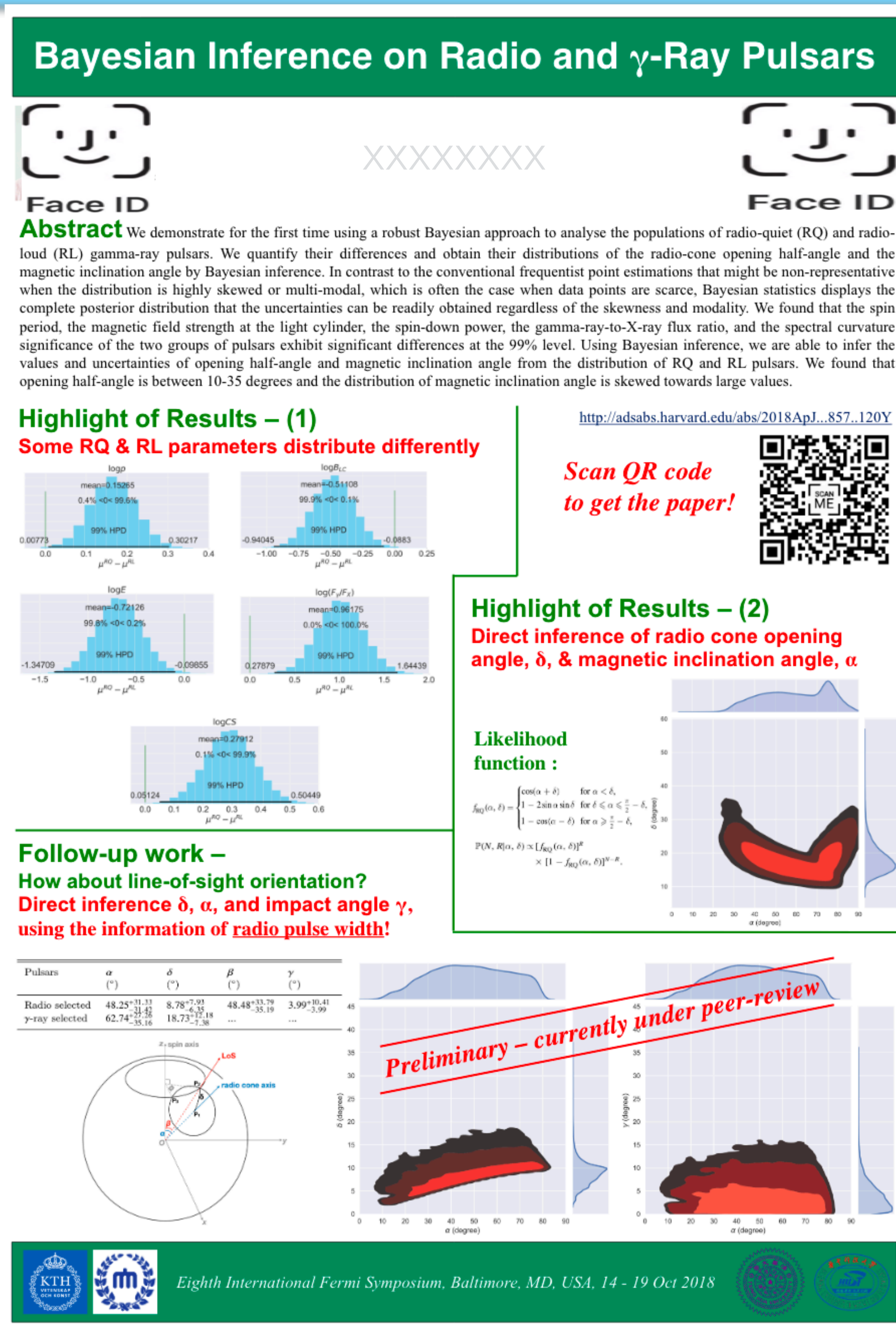

viewgraphs

presentation layout

- do not present more than a few results/conclusions
  - too dense presentations cannot be memorised

“Information overload is a symptom of our desire to not focus on what's important. It is a choice.”
Brian Solis

- outline slide or outline ruler possible,
  but not essential if good logical flow and transitions

- count typically 1 to 2 minutes per slide

- finish with a “take home points” slide

“distringit librorum multitudo”
the abundance of books is distraction
Seneca

text & jargon

- text goals:
  - highlight key points
  - help the audience to get back on track if loss of attention
- text layout
  - no sentences, but bullets
  - **remove words until loss of content**

one cannot read & listen

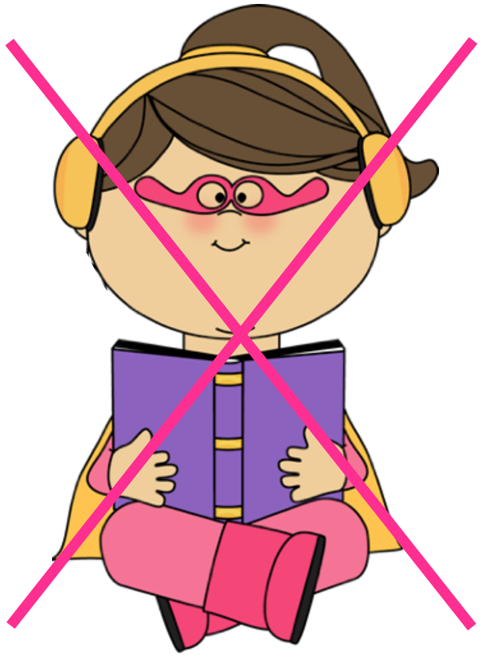

- do others know what I mean ?
  - avoid acronyms, use only well-known ones
  - **define any jargon**

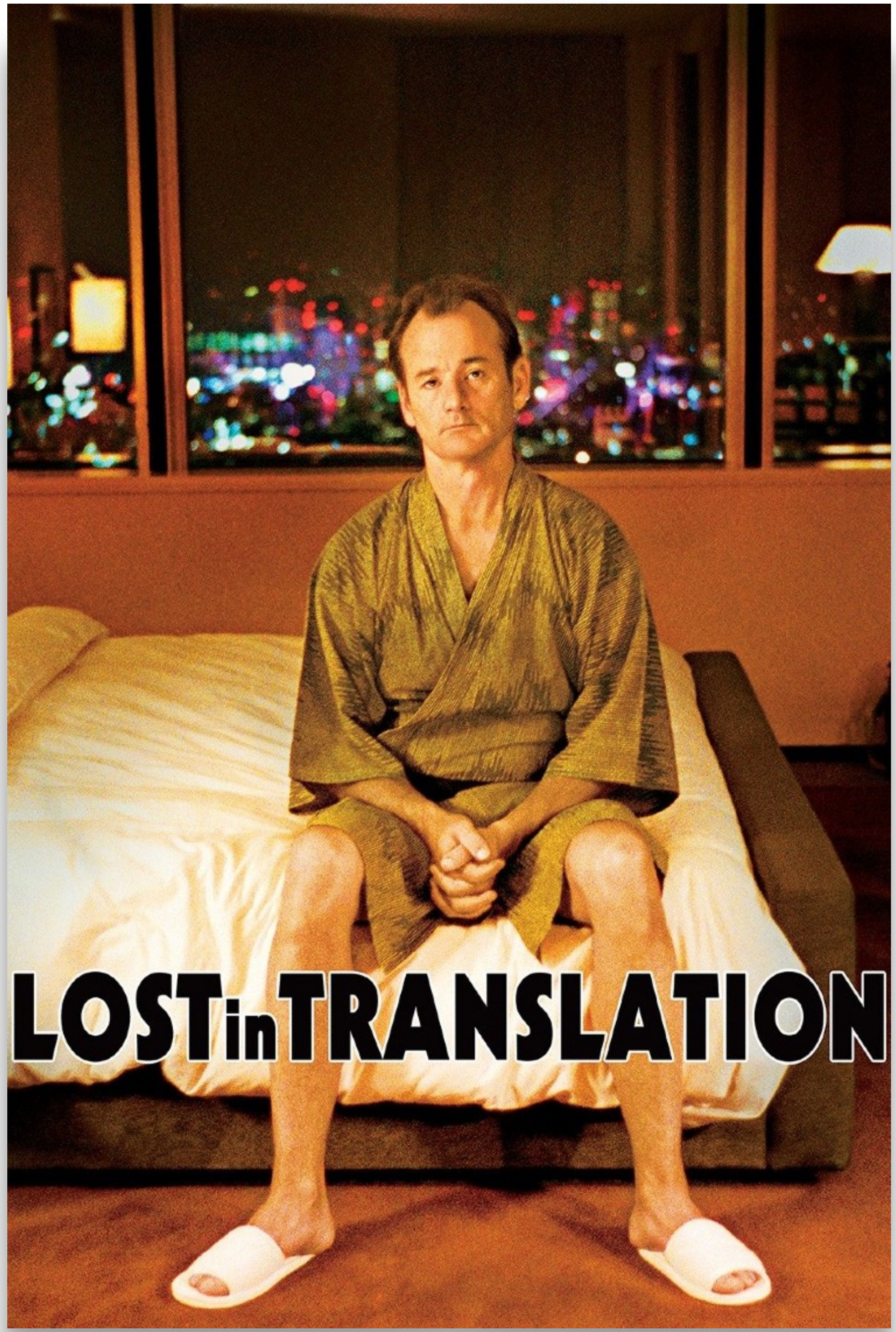

viewgraph layouts

- plots
  - ≤ 2 per viewgraph, rarely 3
  - axes: use visible fonts and **describe their content** !
  - plot references
    - add them for all published plots
    - overlay "preliminary" on unpublished plots
  - colour scales
    - projector test prior to presentation
    - account for colour-blind people
    - optimise the slide background

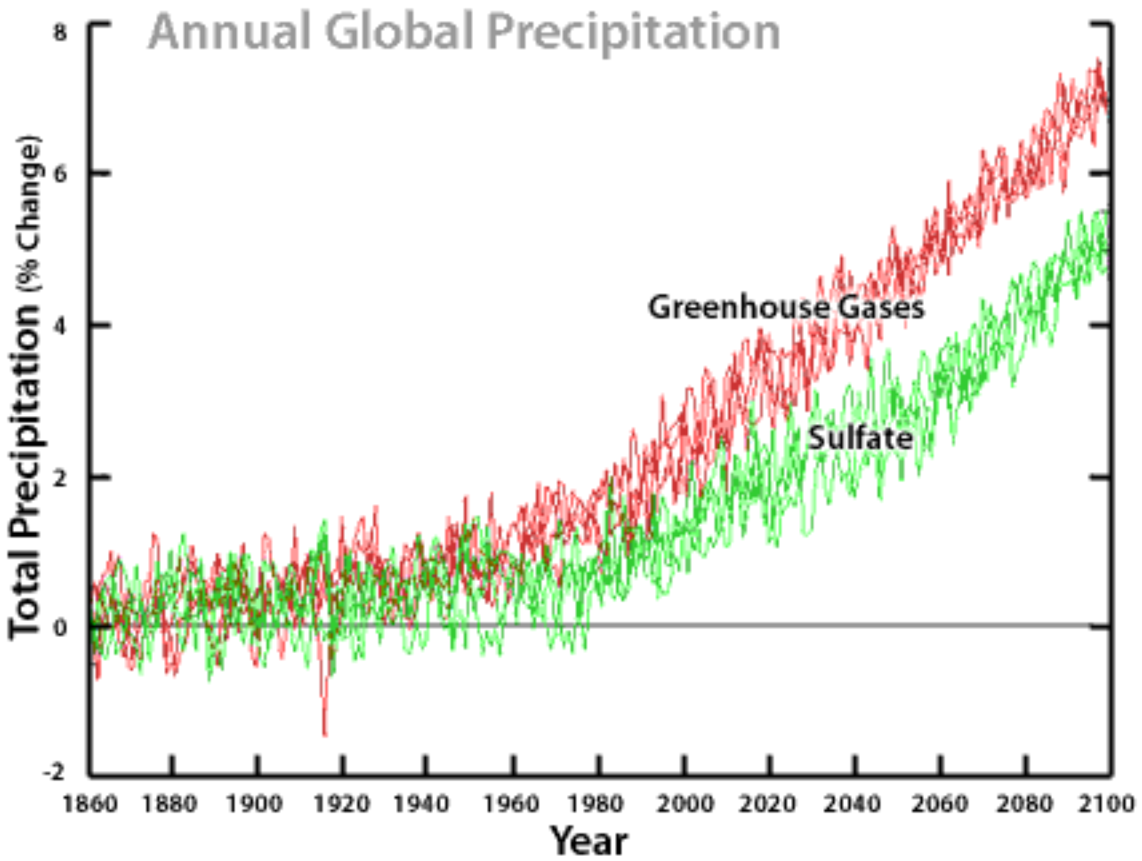

International panel of climate change

- animations: use sparingly in short talks
  - don't loose time with items appearing in sequence (impractical to answer questions)

example

- not up-to-the-point text
- confused plot
- unreadable table (what does it bring?)

Linden et al....

- Linden, T. *et al* (Phys. Rev. D 96, 103016). Pointed out that HAWC sees nearby high flux pulsars.
- Should see more.
- Notes that the TeV signature is a large (~10pc), spatially distinct from the SNR and from the X-ray PWN shock.
- Coined term “TeV Halo” to these objects and suggested the size is a compromise between diffusion of PWN accelerated ~10-100 TeV electron cooling time.
- Middle-age Pulsars (100-400ky) should all be “Geminga-like”
- Suggests that HAWC could even identify un-aligned Pulsars that are poorly aligned for radio detection.

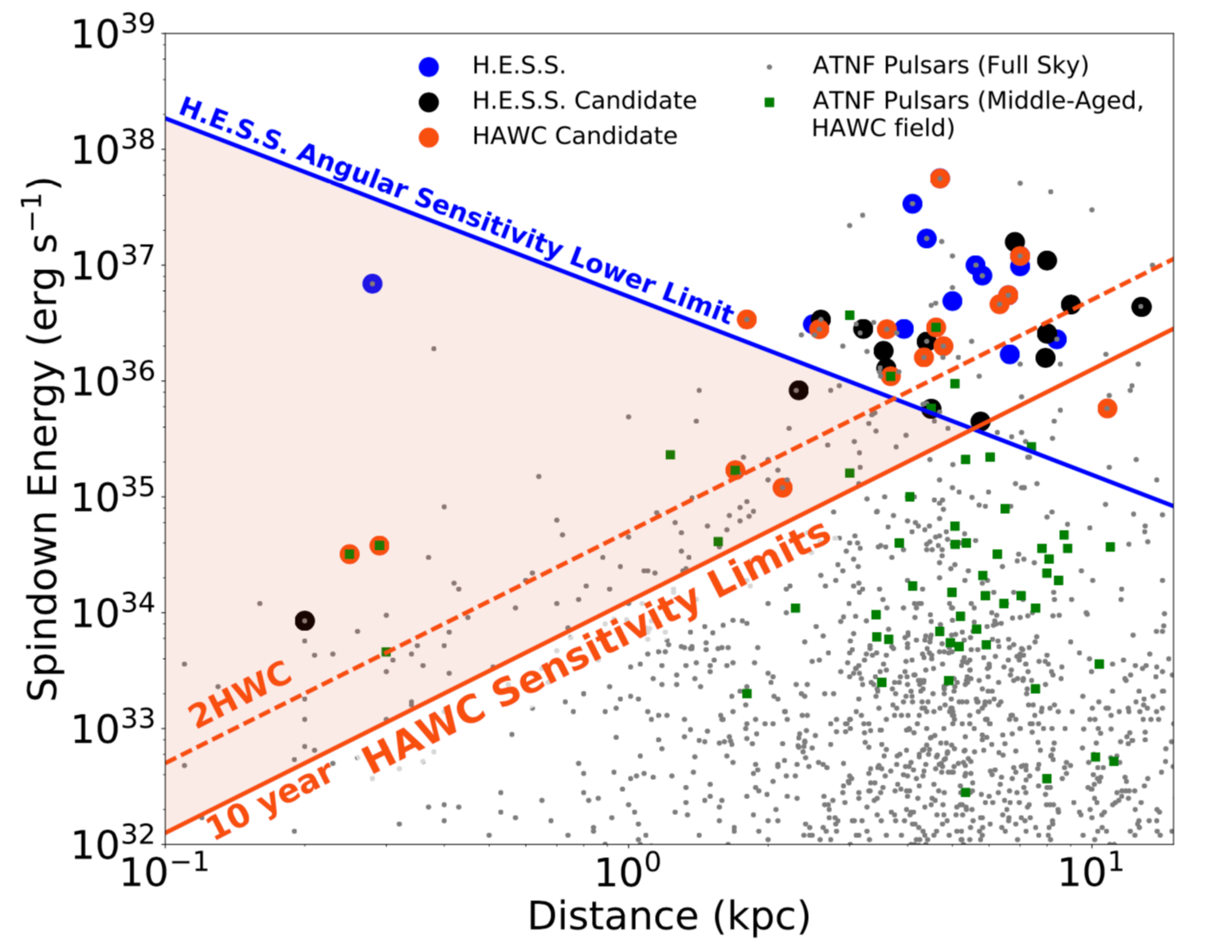

ATNF Name	Dec. (°)	Distance (kpc)	Age (kyr)	Spindown Lum. (erg s^{-1})	Spindown Flux (erg s^{-1} kpc^{-2})	2HWC
J0633+1746	17.77	0.25	342	3.2e34	4.1e34	2HWC J0631+169
B0656+14	14.23	0.29	111	3.8e34	3.6e34	2HWC J0700+143
B1951+32	32.87	3.00	107	3.7e36	3.3e34	—
J1740+1000	10.00	1.23	114	2.3e35	1.2e34	—
J1913+1011	10.18	4.61	169	2.9e36	1.1e34	2HWC J1912+099
J1831-0952	-9.86	3.68	128	1.1e36	6.4e33	2HWC J1831-098
J2032+4127	41.45	1.70	181	1.7e35	4.7e33	2HWC J2031+415
B1822-09	-9.58	0.30	232	4.6e33	4.1e33	—
B1830-08	-8.45	4.50	147	5.8e35	2.3e33	—
J1913+0904	9.07	3.00	147	1.6e35	1.4e33	—
B0540+23	23.48	1.56	253	4.1e34	1.4e33	—

example

- synthetic text
- too small plots
- unreadable axes and labels
- conclusions lost among plots

- More data (6.5 yrs P8 >0.25 GeV), more galaxies, redshift tomography

→ Higher detection significances (e.g., ~12σ for SDSS-DR12, ~11σ for WIxSC)

- CC varies by catalog, energy range, and redshift

→ sources with different properties contribute differently to UGRB

Stay tuned…

- Spectrum shows hints of an energy break

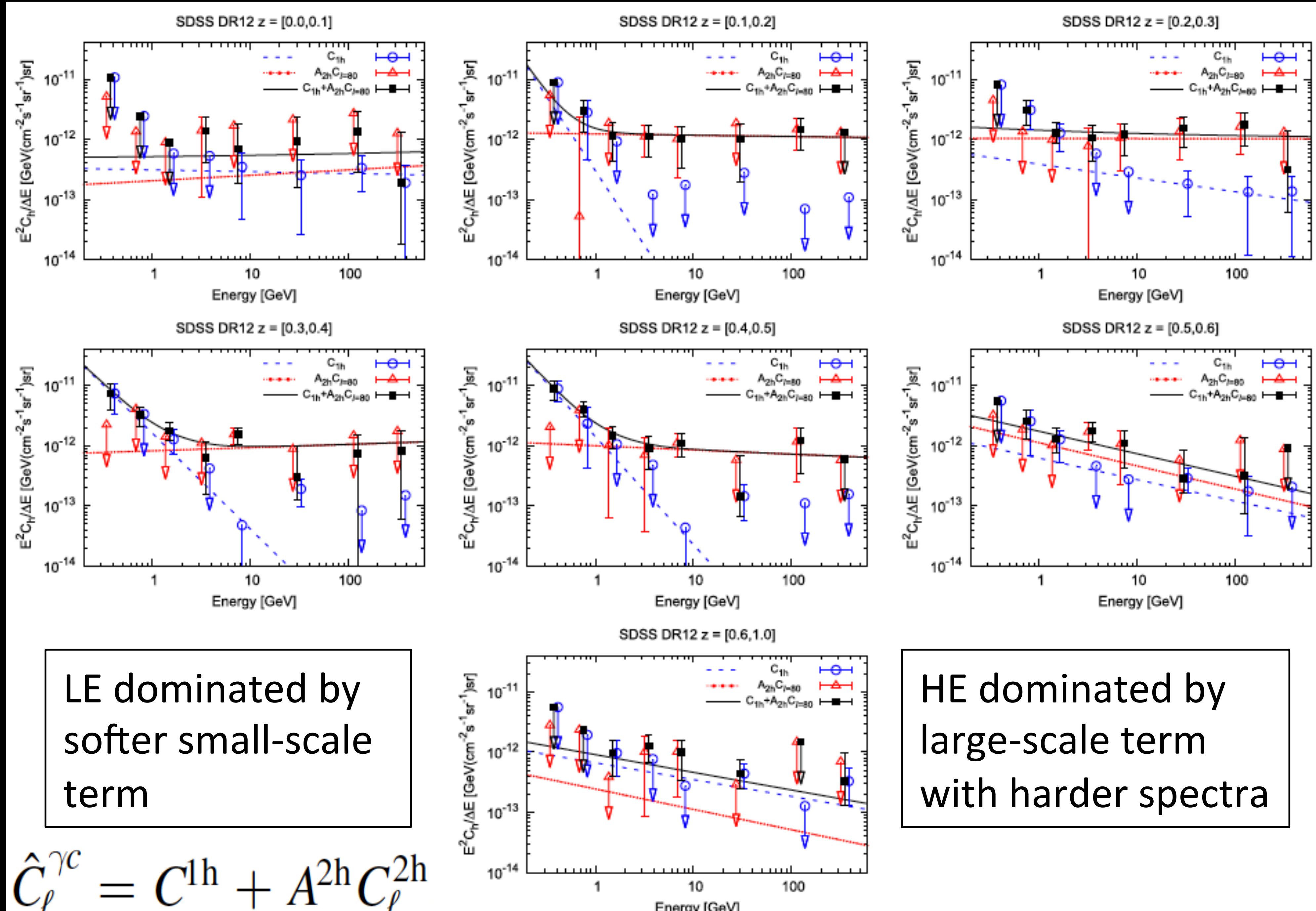

LE dominated by softer small-scale term

HE dominated by large-scale term with harder spectra

$$\hat{C}_\ell^{\gamma c} = C^{1h} + A^{2h} C_\ell^{2h}$$

example

- attractive layout, but remove white frame
- red/blue contrast invisible, axes too

Analysis with real data

Canada-France-Hawaii Lensing Survey (CFHTLenS)

- Four patches, total ~154 deg^2
- 11 resolved galaxies per arcmin^2
- Photo-z between 0.2 < z < 1.3 (median 0.75)
- About 5.7 million galaxies

Fermi-LAT

- Approx 5 yrs of Pass 7REP data
- 1 – 500 GeV ULTRACLEAN photons
- Treat patches independently

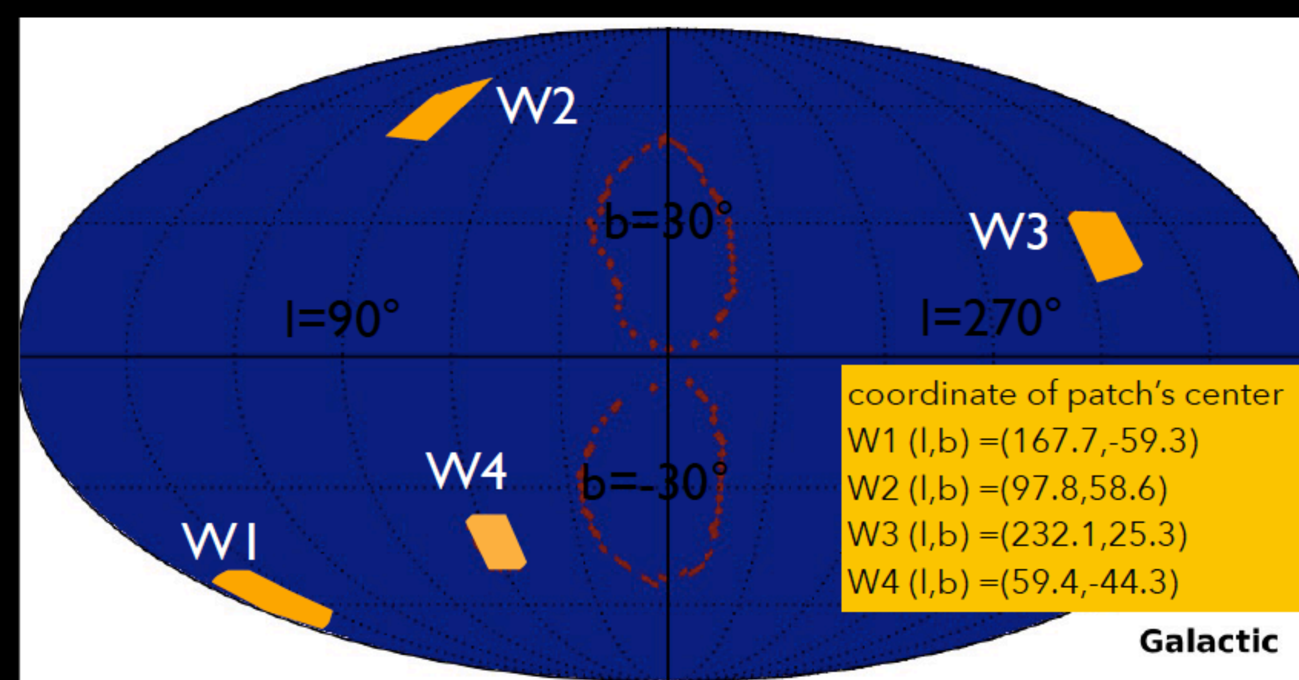

example

- clear plot
- synthetic text
- highlighting improvement
- missing plot reference

This work

- Use 9 years of P8 LAT data
- 739 blazars + 1 GRB
- Measure intrinsic spectrum (τ<0.1) and extrapolate
- Perform a time-resolved analysis
- Analysis optimized on simulations

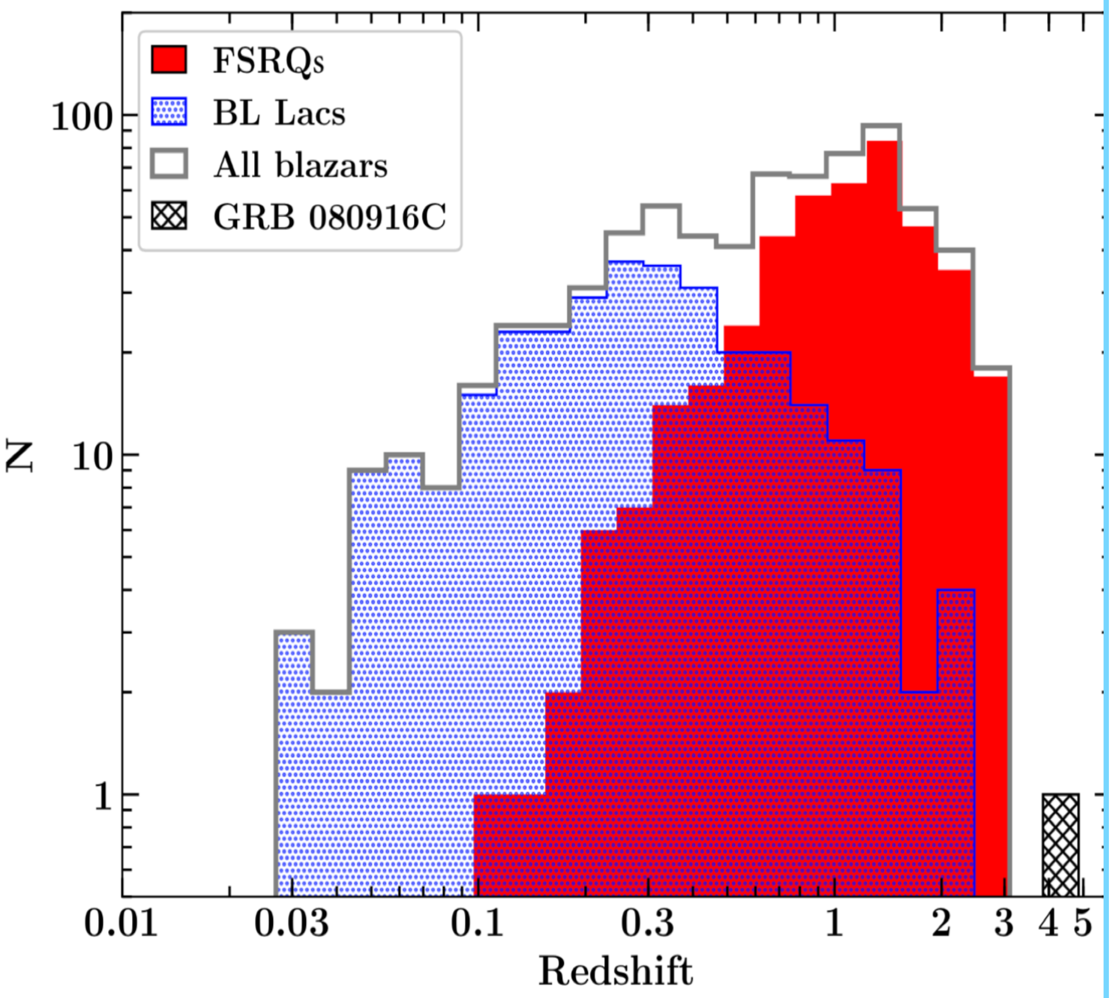

Analysis improved over the Ackermann+12 results

oral presentation

- learn by heart
  - 1 or 2 key sentences for each side, delivering the key information about the slide (should include the keywords present on the slide)
  - how to transition from one slide to the next
  - the rest of the talk will flow naturally

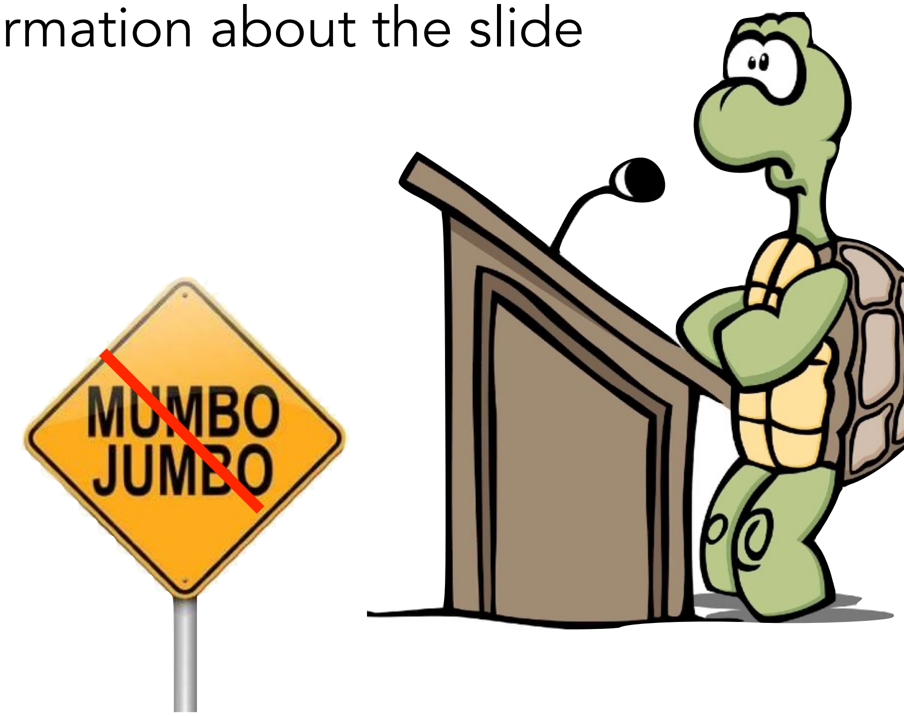

- make eye contact with the audience
  - turn to slides only to point at plots (and to help your memory)
- spare time for questions
  - leave the "take-home points" slide on the screen while answering questions
  - turn to the chairperson for help if you don't understand the question
  - prepare backup slides to answer likely questions

Figure tips

illustrate key points

- make use of the photographic memory of the spectator
- eau = 0.2 ± x % de la masse

make didactic plots

- take a publicist look at your publication plots

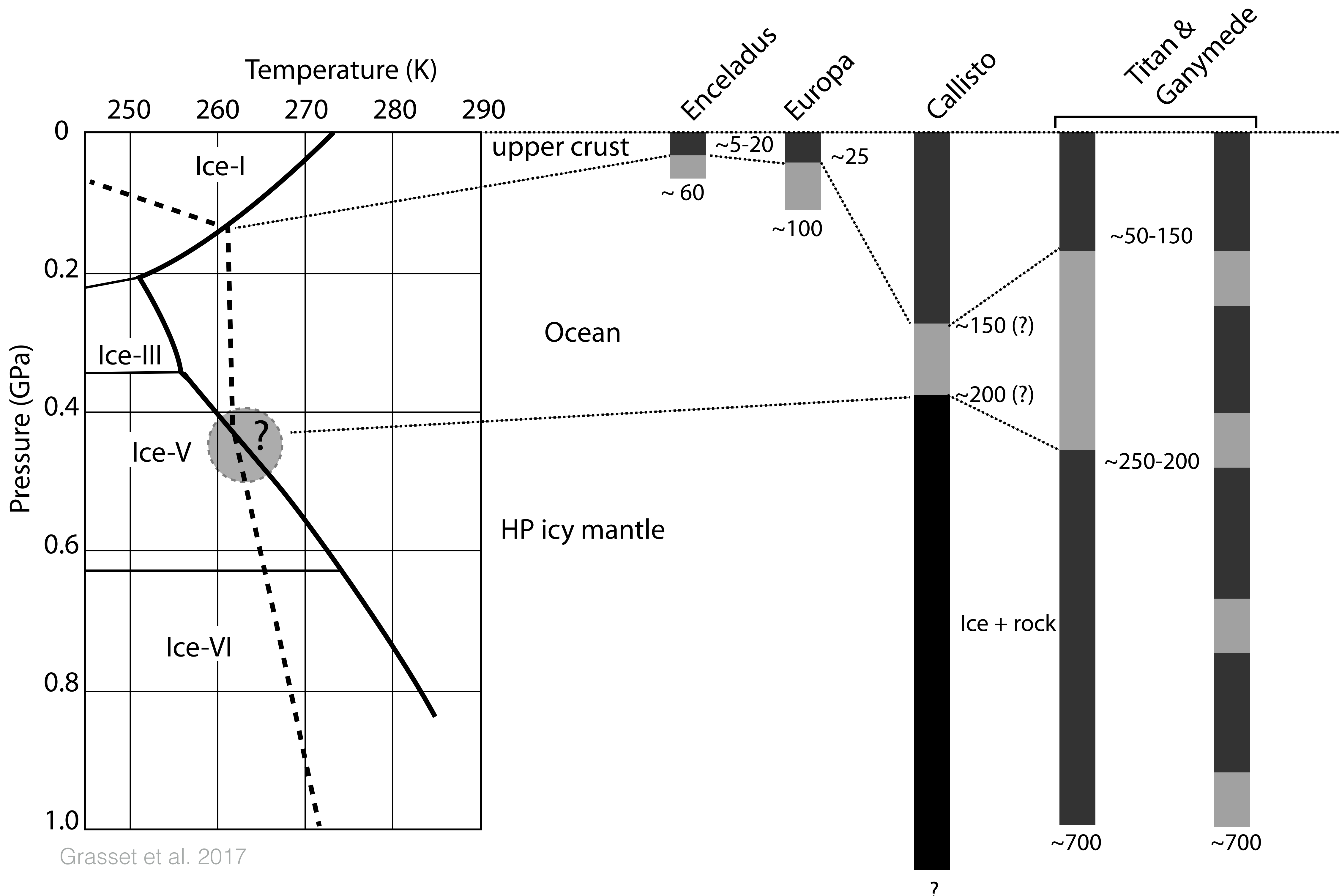

Grasset et al. 2017

self-explanatory plots

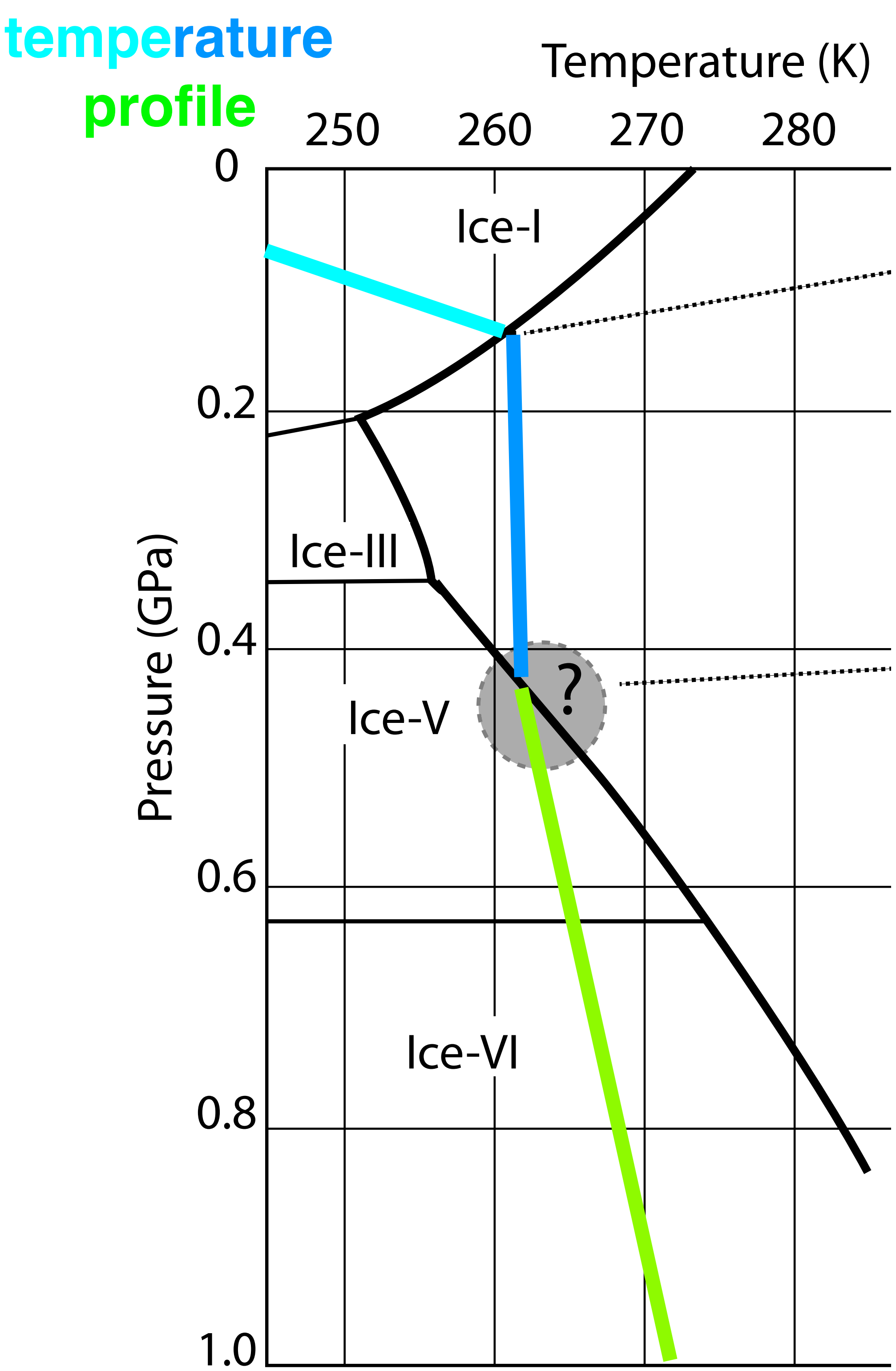

Grasset et al. 2017

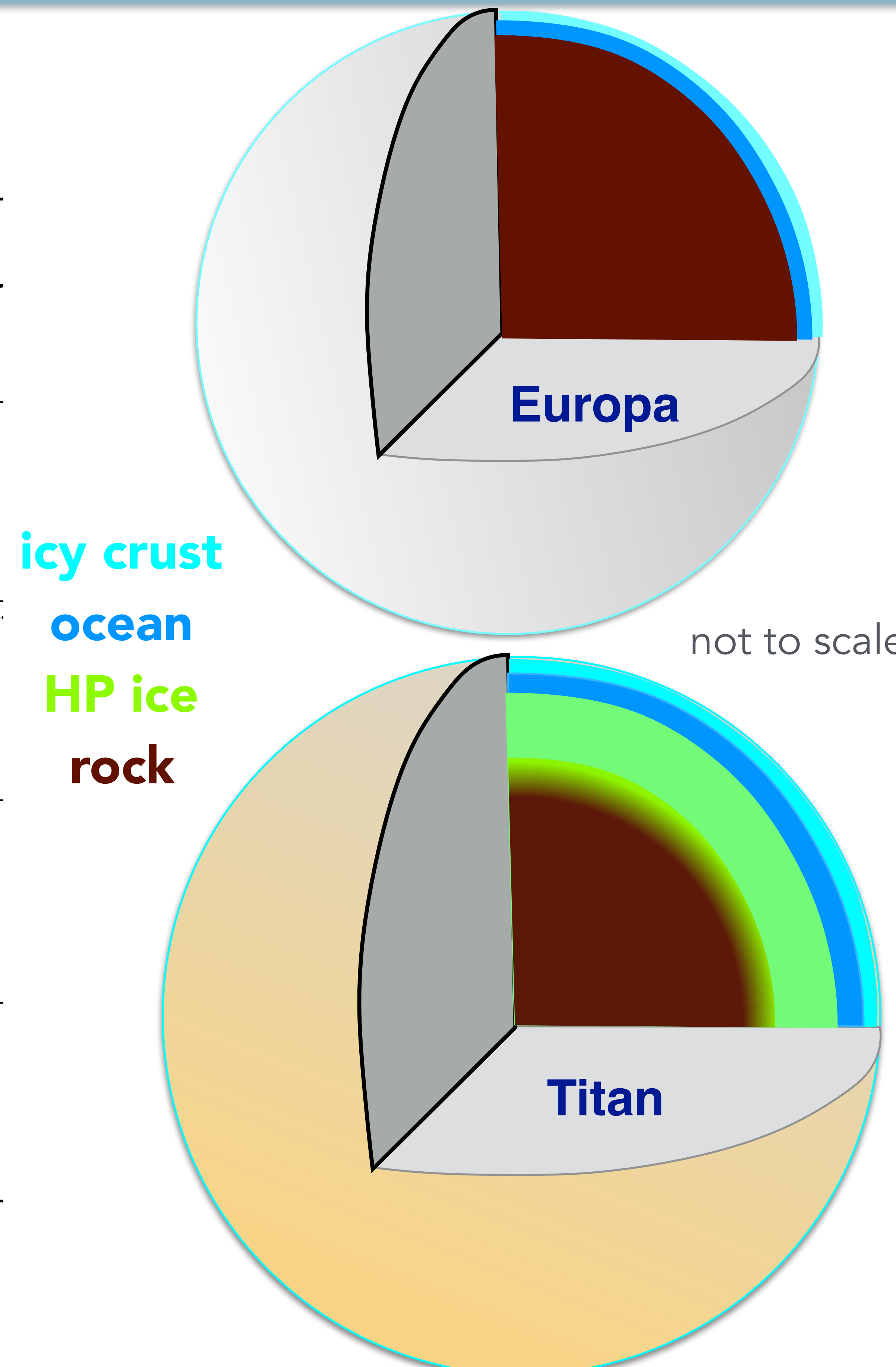

Novel: Open Observatory

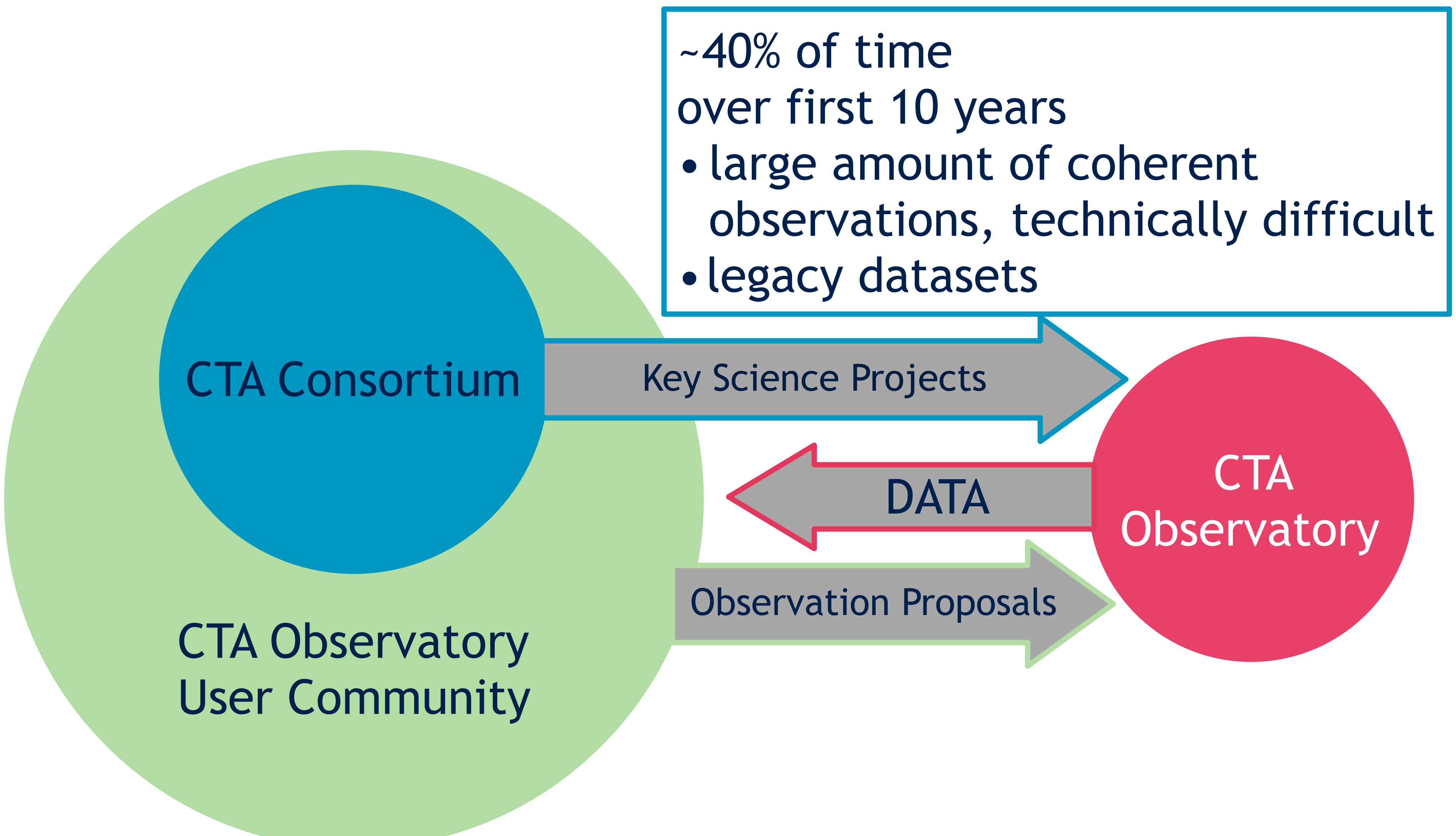

synthetic flow charts

- beware of redundant text

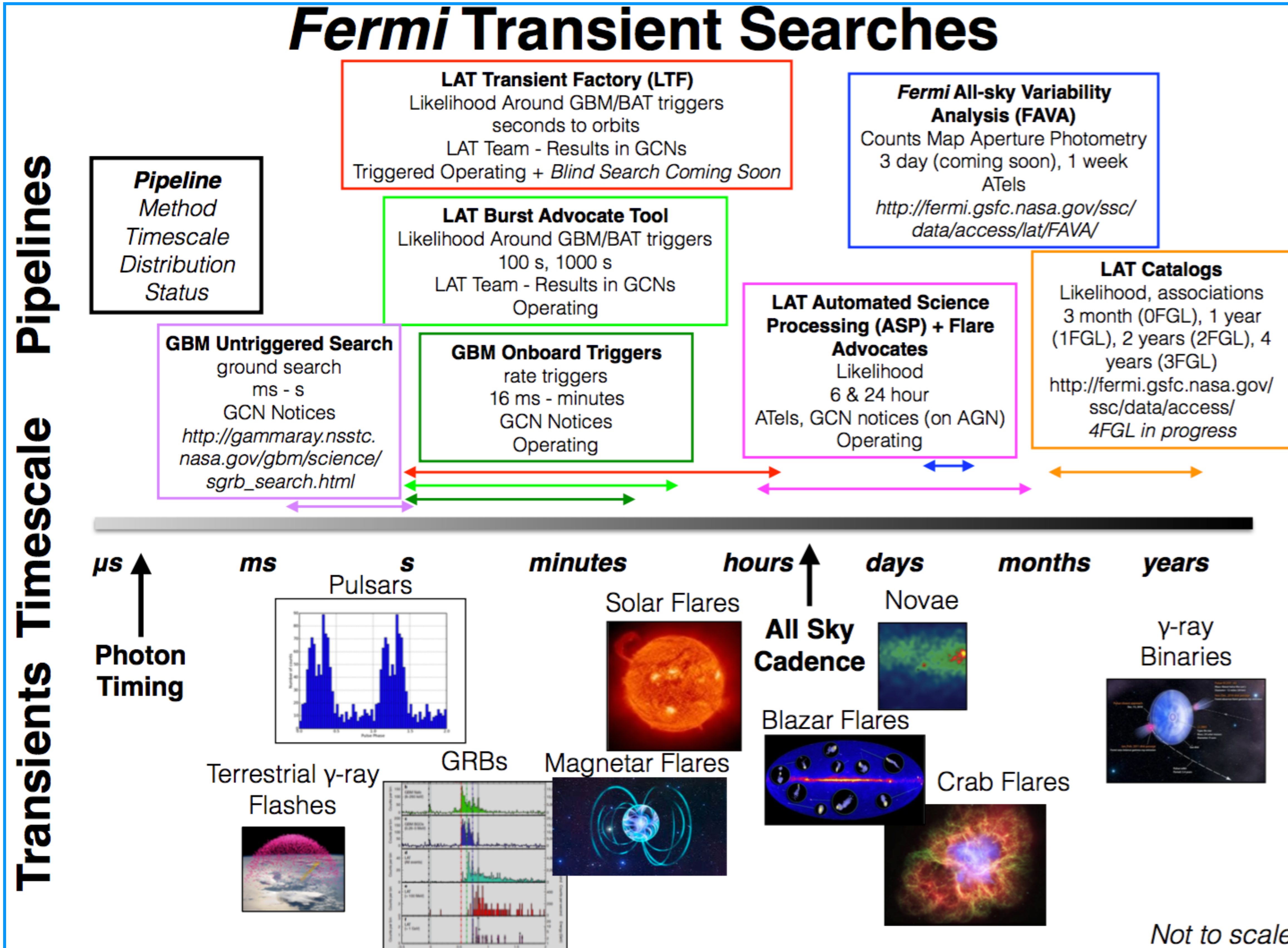

improve scatter plots

- using 2D or 3D histos

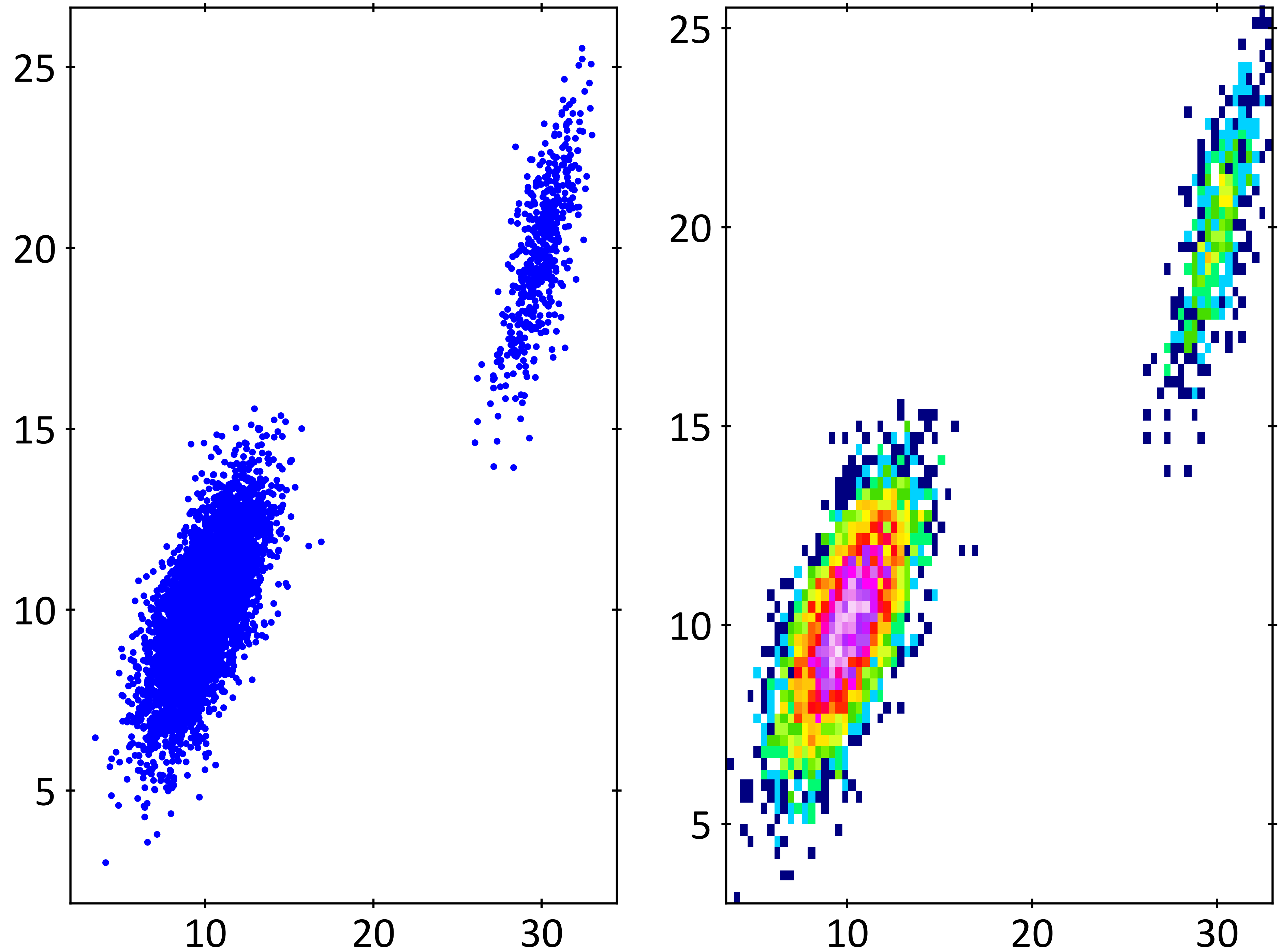

choose background

- light intensity highlights small scales and sharp gradients

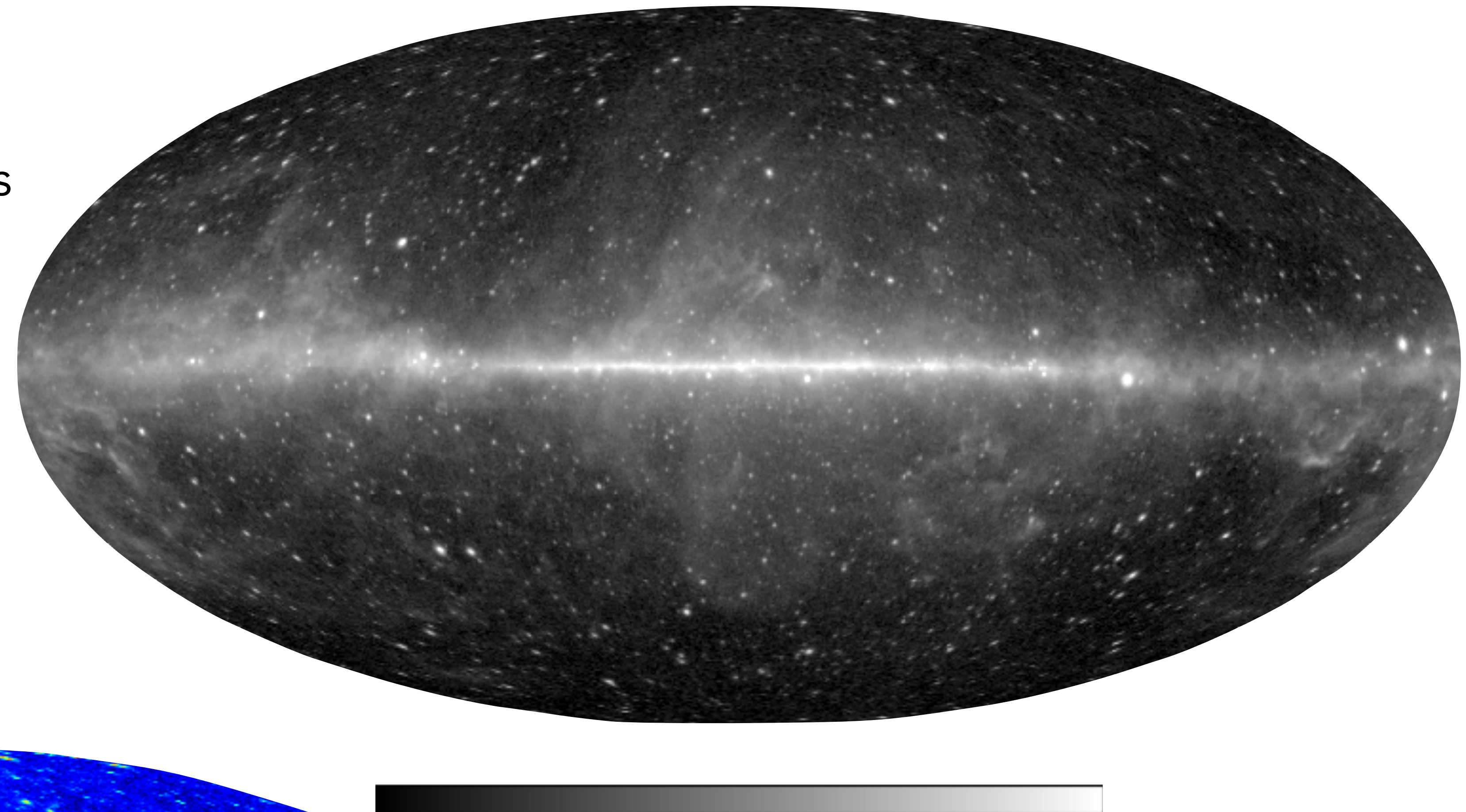

- colour highlights large scales

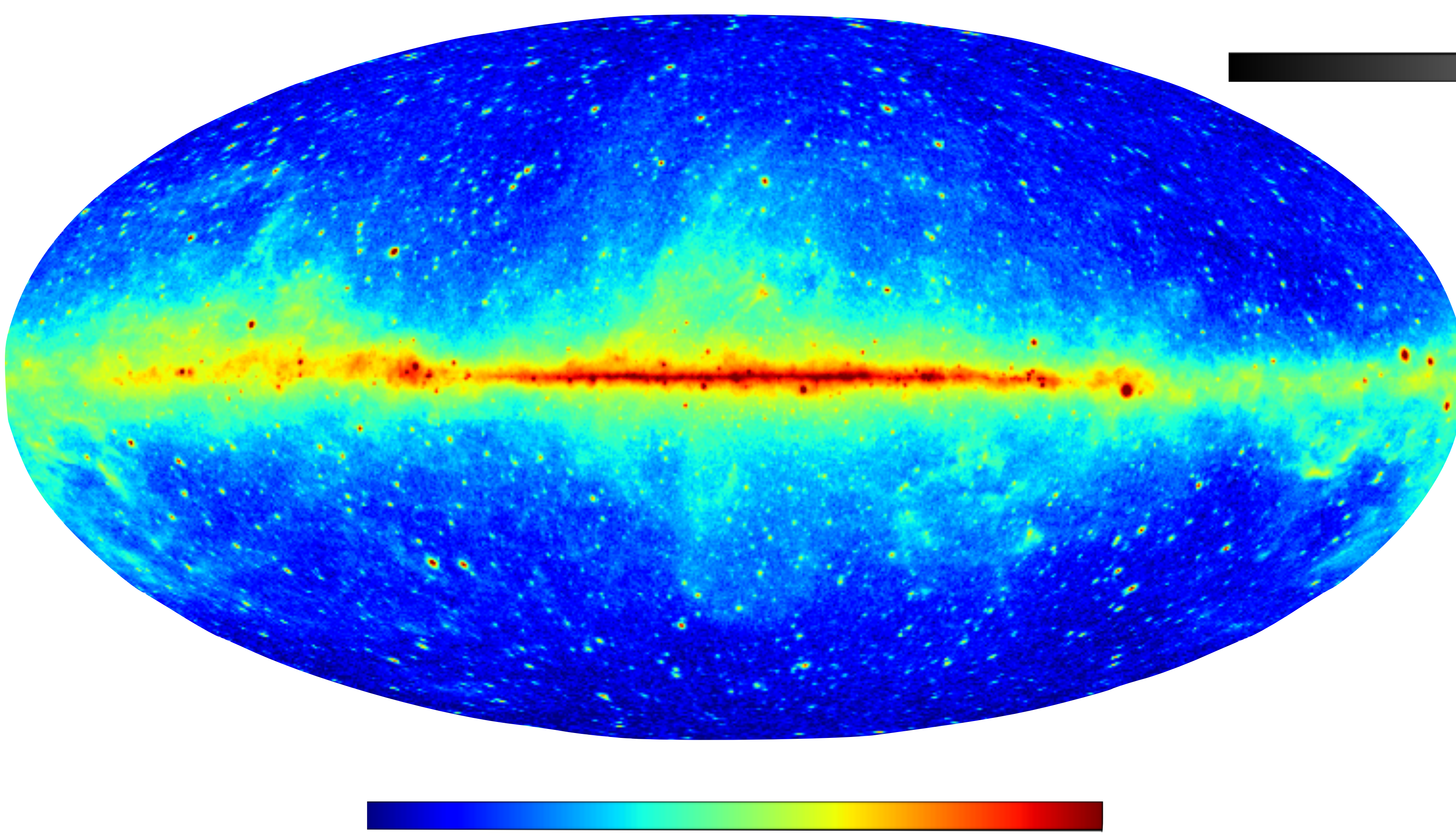

colour scales

- light intensity highlights small scales and sharp gradients

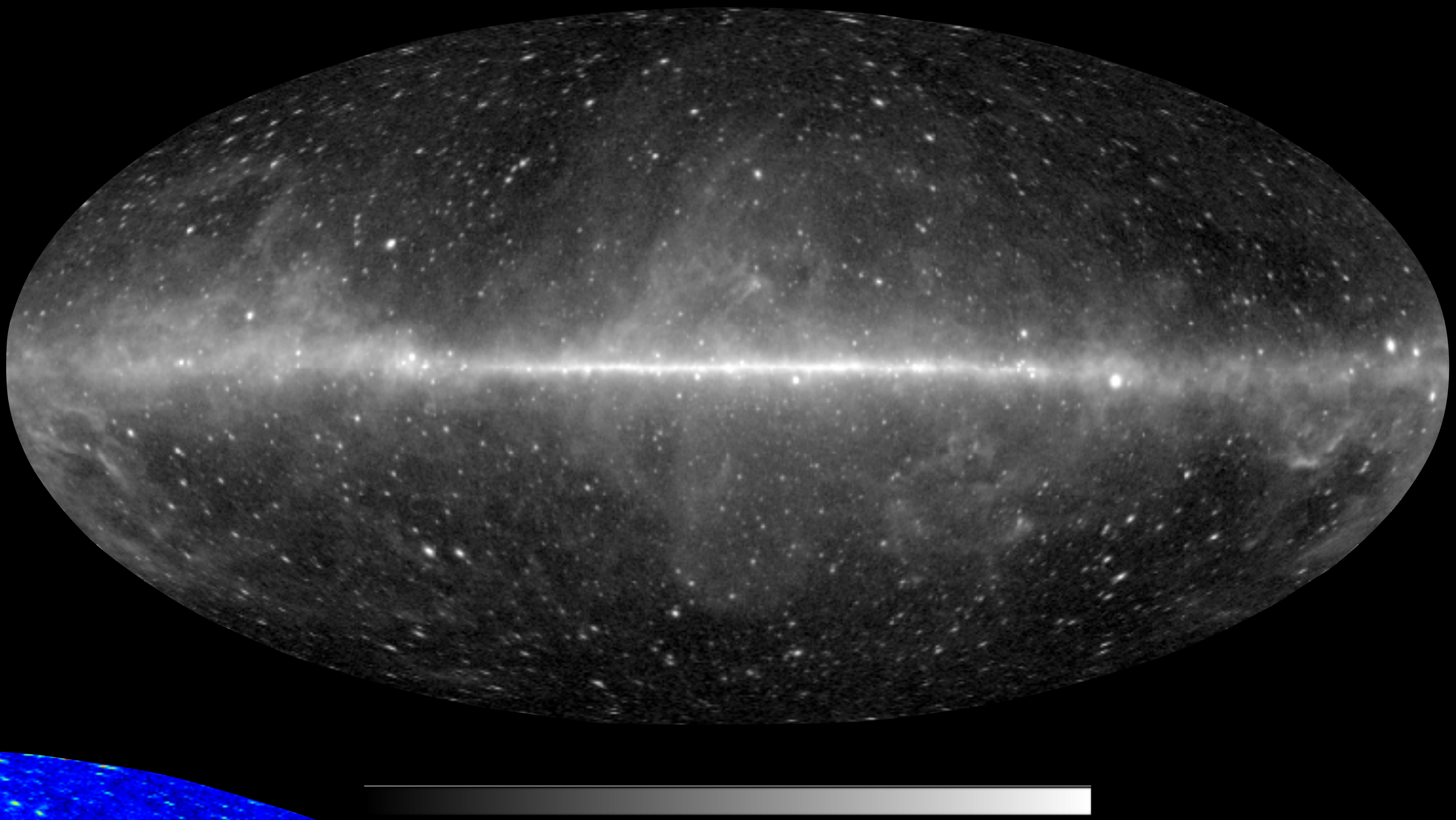

- colour highlights large scales

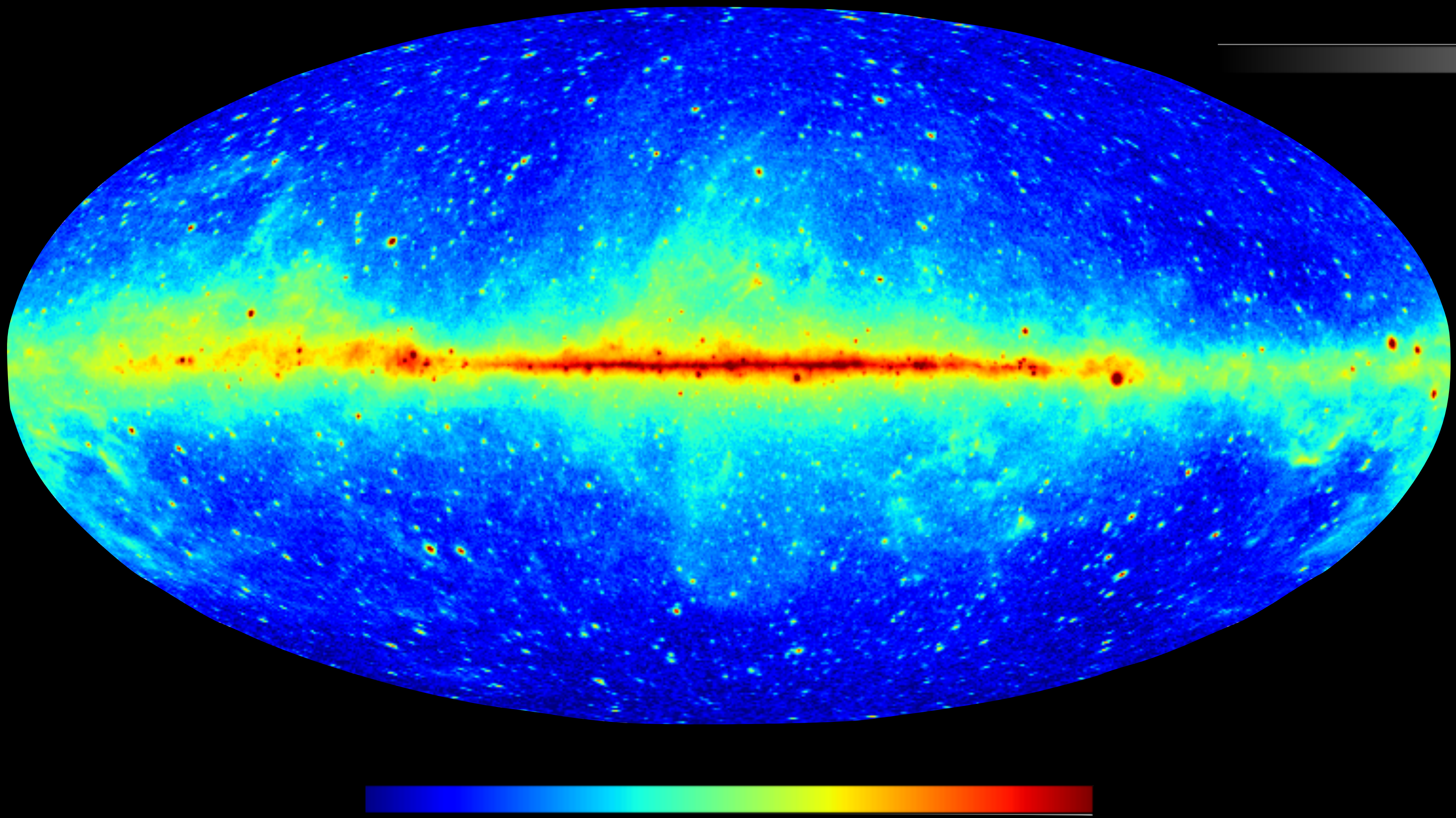

colour scales

- alternate dark & light colours for complex structures

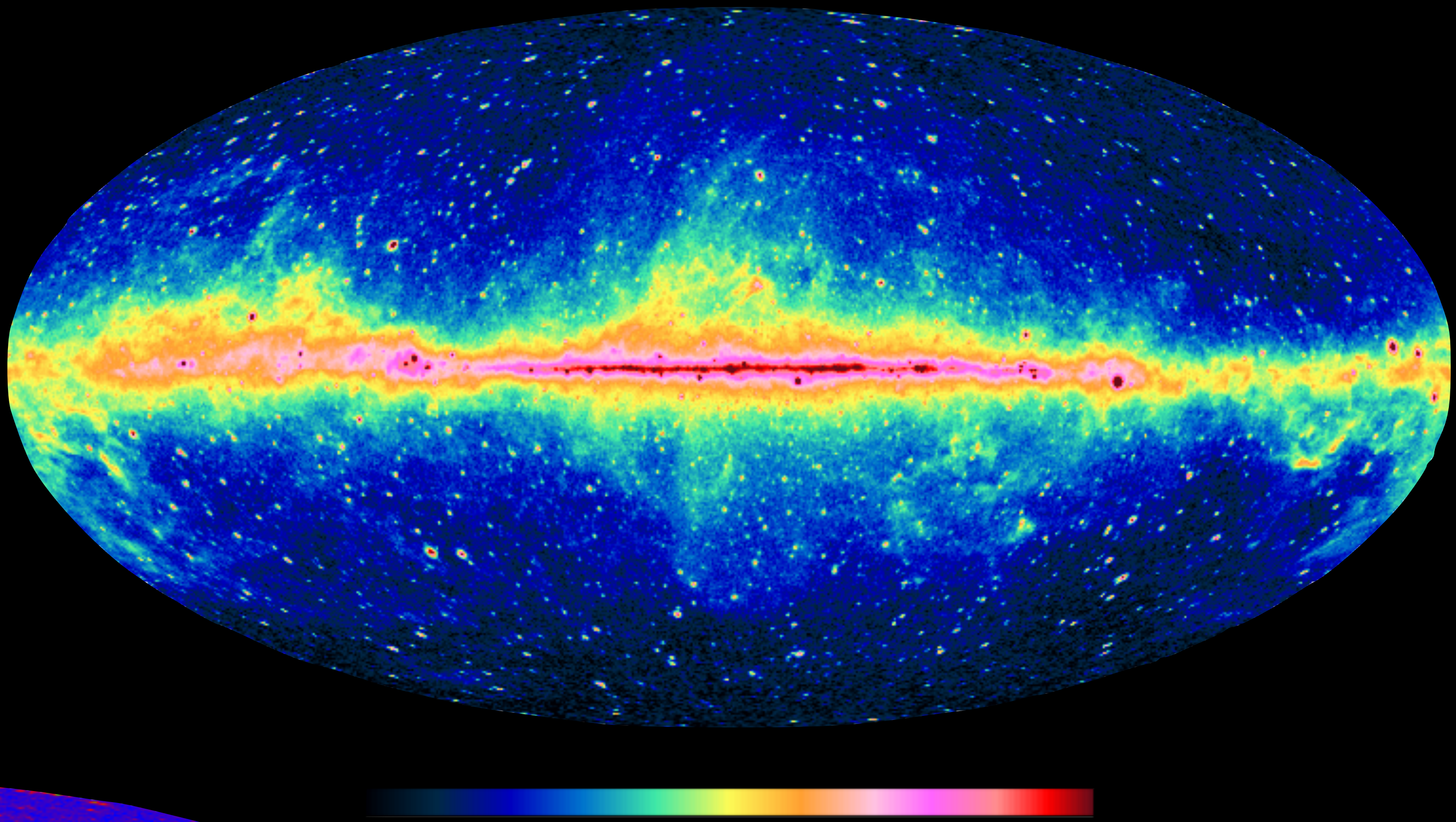

- avoid red vs blue !

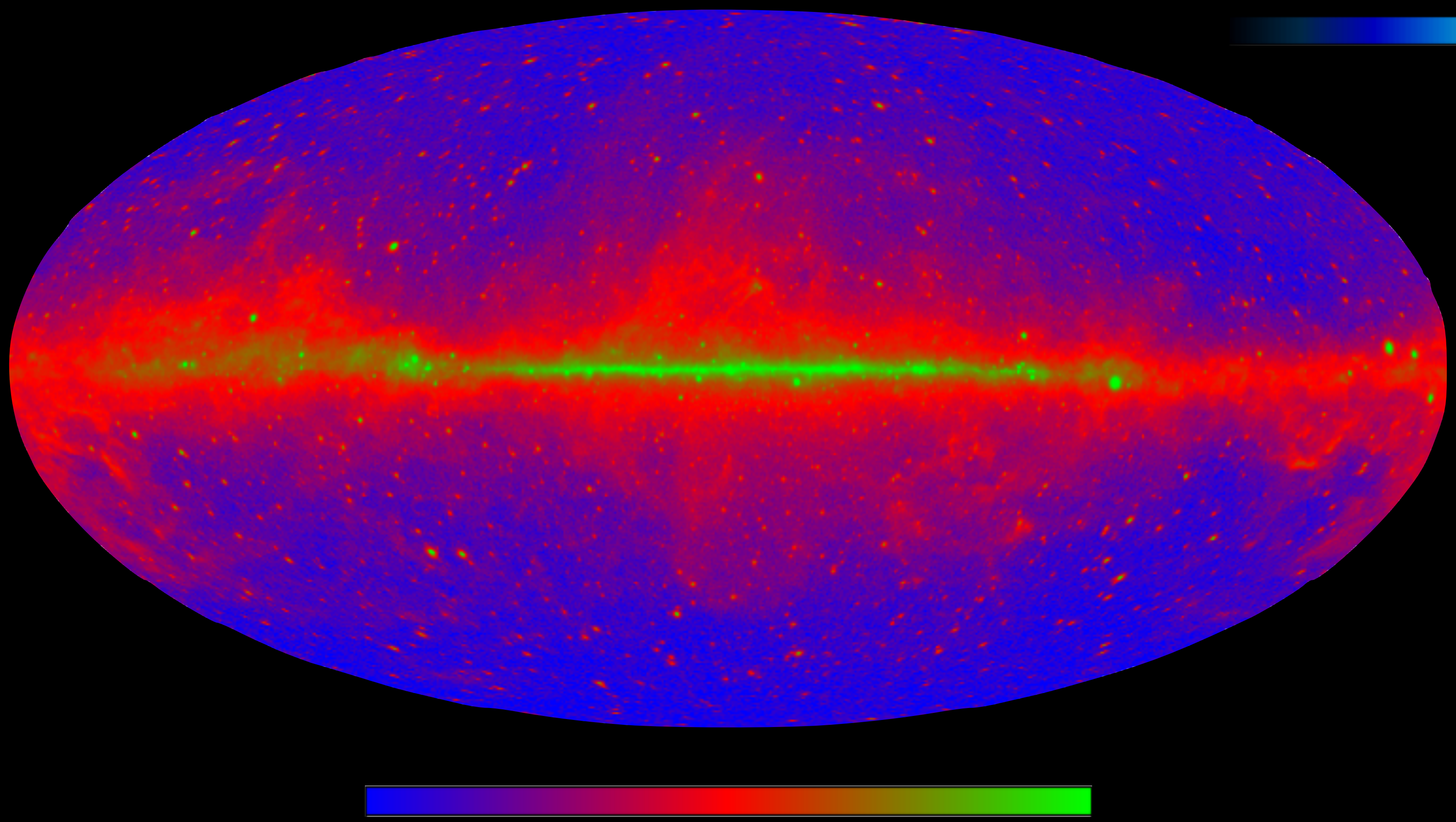

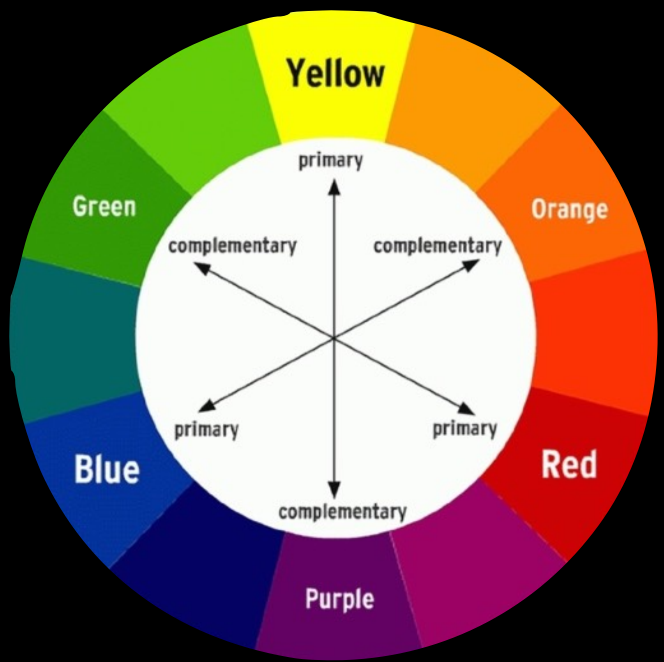

do you see Maxwell's equations?

- comment the role of the different equation terms !

$$\nabla \cdot \vec{E} = \frac{\rho}{\epsilon_0}$$

$$\nabla \cdot \vec{B} = 0$$

$$\nabla \times \vec{E} = -\frac{\partial \vec{B}}{\partial t}$$

$$\nabla \times \vec{B} = \mu_0 \left(\vec{j} + \epsilon_0 \frac{\partial \vec{E}}{\partial t} \right)$$

$$\nabla \cdot \vec{E} = \frac{\rho}{\epsilon_0}$$

$$\nabla \cdot \vec{B} = 0$$

$$\nabla \times \vec{E} = -\frac{\partial \vec{B}}{\partial t}$$

$$\nabla \times \vec{B} = \mu_0 \left(\vec{j} + \epsilon_0 \frac{\partial \vec{E}}{\partial t} \right)$$

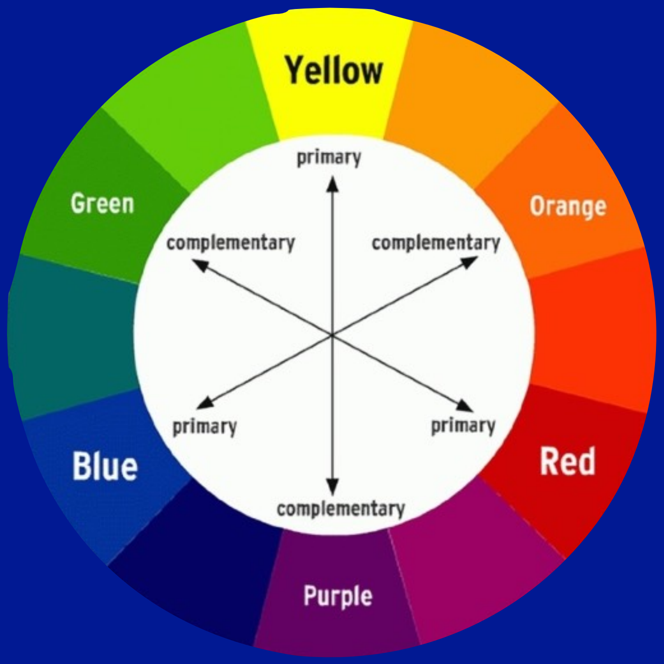

colour blindness

- ~ 8% colour-blind people
- don't rely only on colour to differentiate data

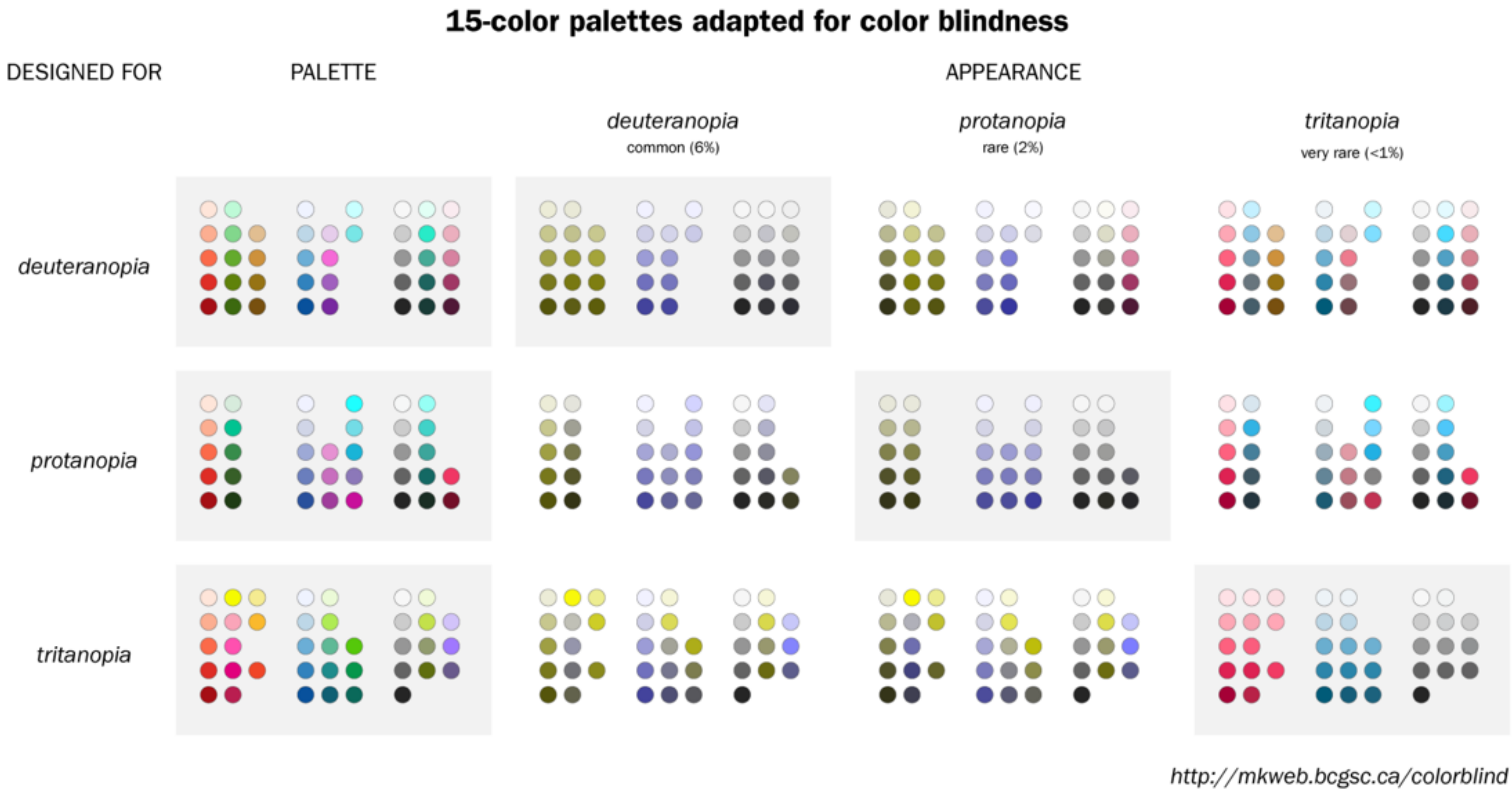

colour-blind friendly plots

- leverage dark vs. light
- use different markers, pie charts,

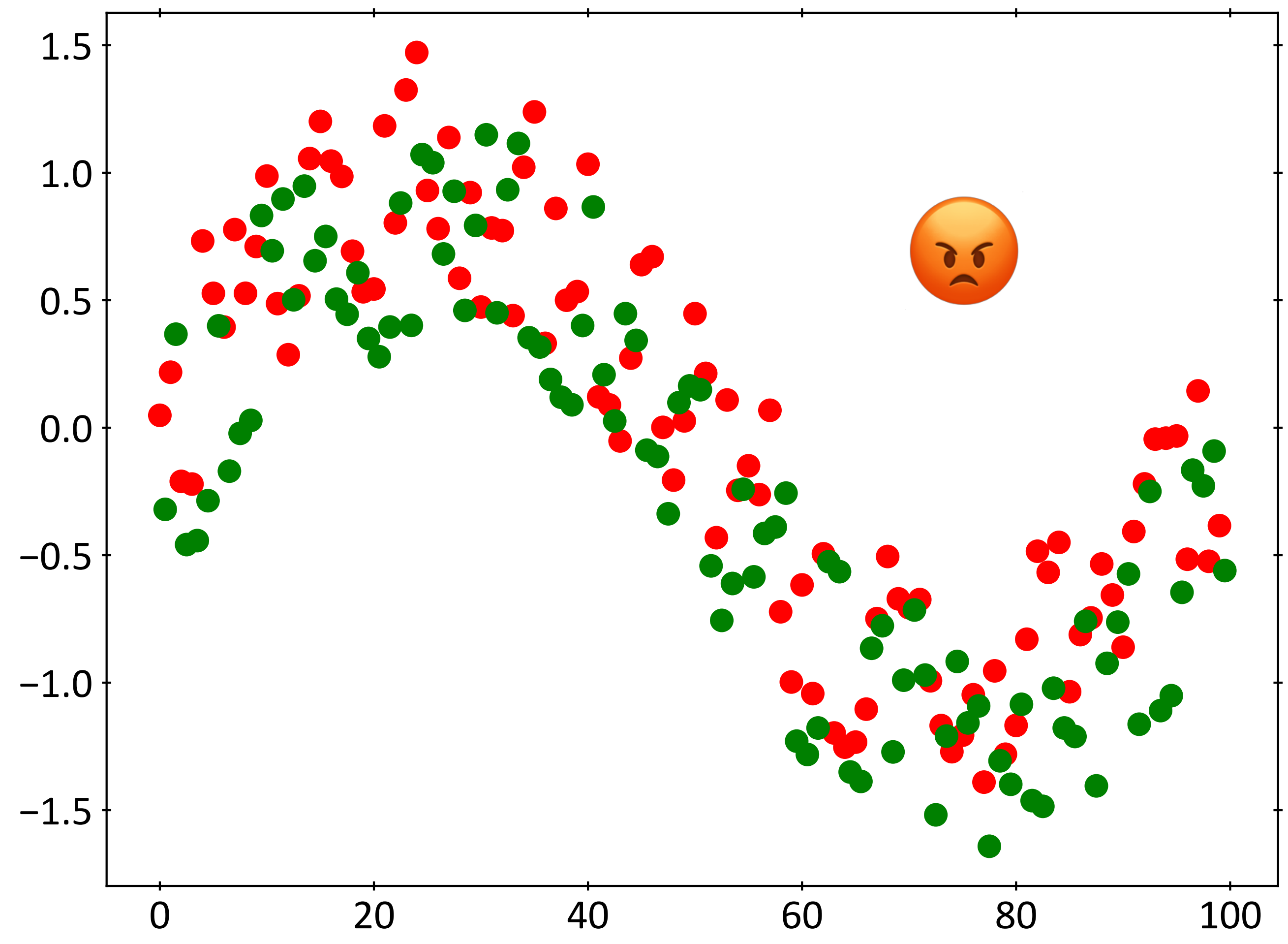

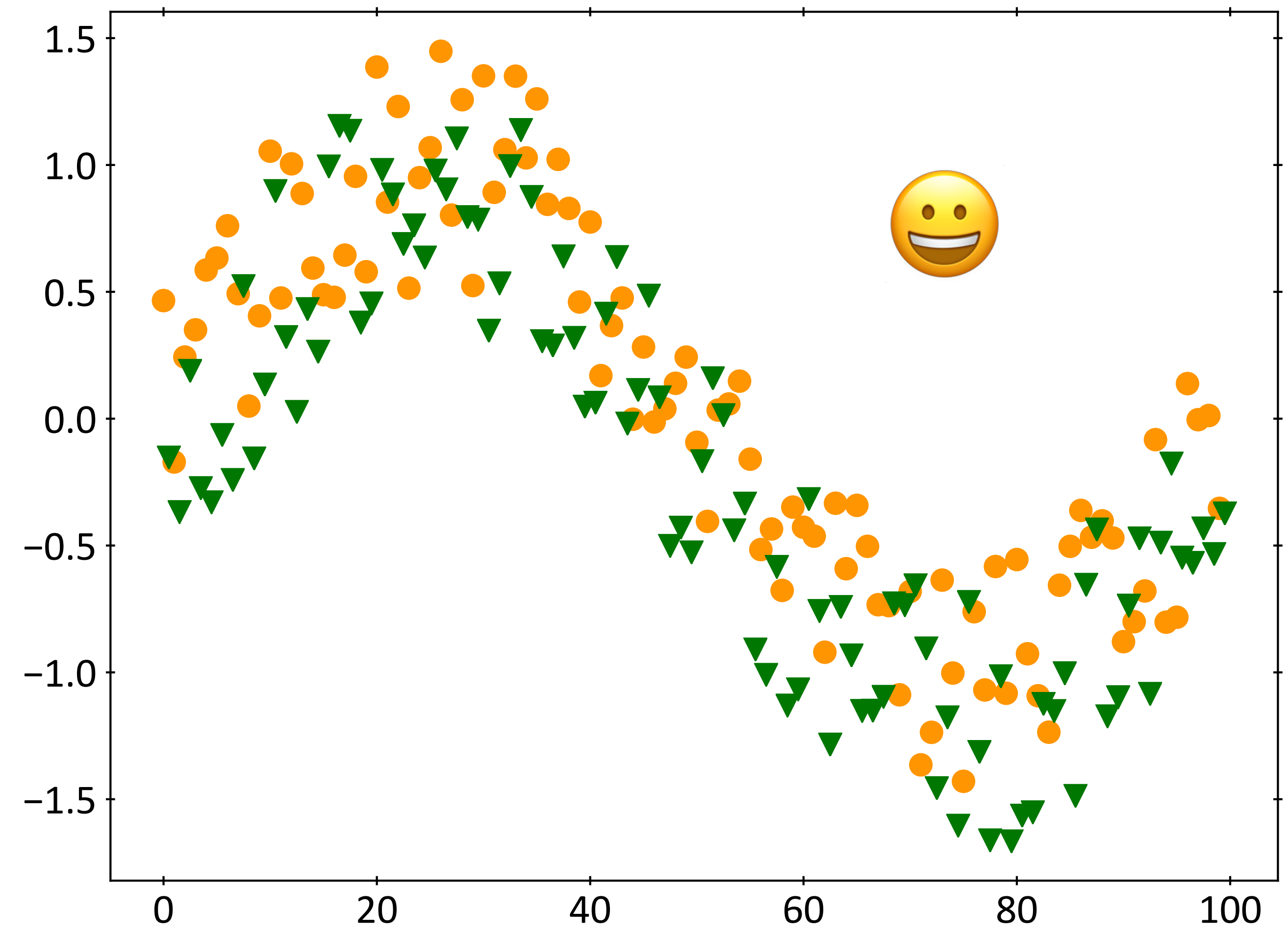

conference goals

conference goals

- prepare a list of people to meet and discuss with (from the program & abstracts)
  - ask your advisor/colleagues to introduce you
- engage in many conversations
  with unknown or foreign colleagues
  - ask questions
  - feel free to say "I don't know" or
    "can you explain"
  - avoid meals with your lab mates
- build contacts
  - ask about projects in other institutes
  - ask about PDA opportunities
- attend the presentations
  - choose talks across parallel sessions
  - listen to the talks, even unrelated to your topic !
  - ideas come unaware !
  - avoid
    - reading/working on your laptop
    - avoid doing your emails

science knowledge builds on crossing information

Keep it simple, keep it light

"Simple can be harder than complex: you have to work hard to get your thinking clean to make it simple. But it's worth it in the end because once you get there, you can move mountains."
Steve Jobs

don't forget
to have fun